Title

Gross primary productivity of a large metropolitan region in midsummer using high spatial resolution satellite imagery

Journal

Urban Ecosystems, 21(5)

ISSN

1083-8155

Authors

Miller, David L
Roberts, Dar A
Clarke, Keith C
et al.

Publication Date

2018-10-01

DOI

10.1007/s11252-018-0769-3

Peer reviewed

Gross primary productivity of a large metropolitan region in midsummer using high spatial resolution satellite imagery

David L. Miller, Dar A. Roberts, Keith C. Clarke, Yang Lin, Olaf Menzer, Emily B. Peters & Joseph P. McFadden

Urban Ecosystems

ISSN 1083-8155
Volume 21
Number 5

Urban Ecosyst (2018) 21:831-850
DOI 10.1007/s11252-018-0769-3

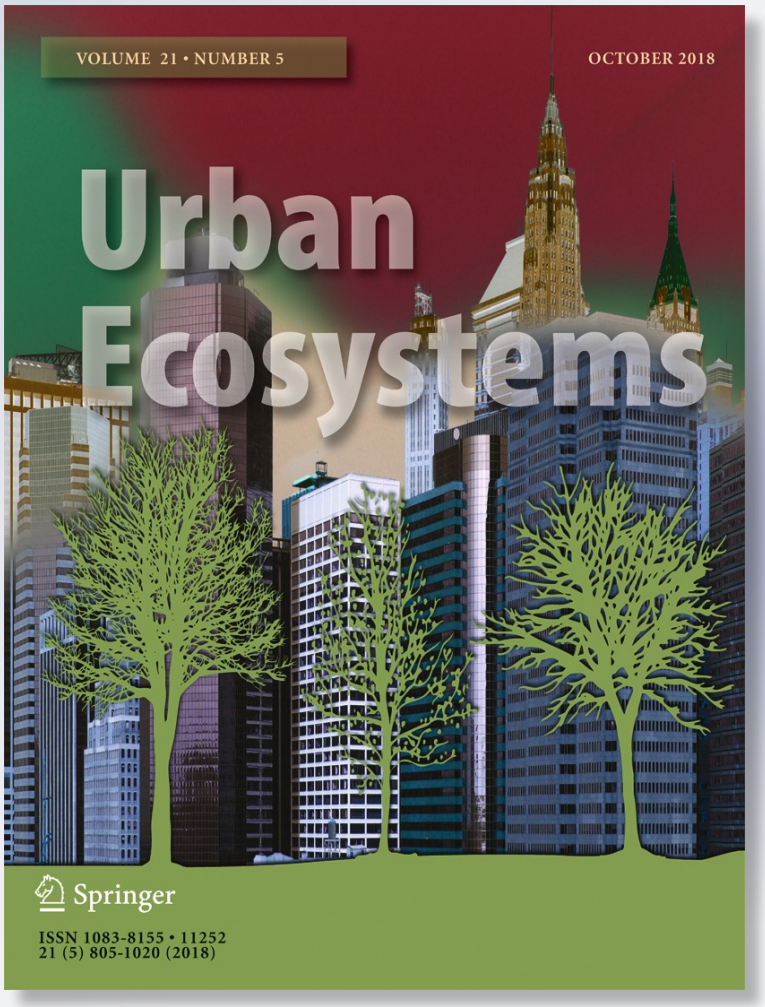

Springer

Urban Ecosystems (2018) 21:831–850
https://doi.org/10.1007/s11252-018-0769-3

Gross primary productivity of a large metropolitan region in midsummer using high spatial resolution satellite imagery

David L. Miller[1] · Dar A. Roberts[1] · Keith C. Clarke[1] · Yang Lin[2] · Olaf Menzer[1] · Emily B. Peters[3] · Joseph P. McFadden[1]

Published online: 11 June 2018

Abstract

Although gross primary productivity (GPP) is estimated with remote sensing over large regions of Earth, urban areas are usually excluded due to the lack of light use efficiency (LUE) parameters for urban vegetation and the spatial heterogeneity of urban land cover. Here, we estimated midsummer GPP, both within and among vegetation and land-use types, across the Minneapolis-Saint Paul, Minnesota metropolitan region. We derived LUE parameters for urban vegetation types using estimates of GPP from tree sap flow and eddy covariance CO_2 flux observations, and from fraction of absorbed photosynthetically active radiation based on 2 m resolution WorldView-2 satellite imagery. Mean GPP per unit land area (including vegetation, impervious surfaces, and soil) was 2.64 g C m^{-2} d^{-1}, and was 4.45 g C m^{-2} d^{-1} per unit vegetated area. Mapped GPP estimates were within 11.4% of estimates from independent tall tower eddy covariance measurements. Turf grass GPP had a larger coefficient of variation (0.18) than other vegetation classes (~0.10). Vegetation composition was largely consistent across the study area. Excluding golf courses, mean land-use GPP for the total study area varied more by percent vegetation cover ($R^2 = 0.98$, $p < 0.001$) than by variability within vegetation classes ($R^2 = 0.21$, $p = 0.19$). Urban GPP in general was less than half that of natural forests and grasslands in the same climate zone.

Keywords Primary production · Carbon cycle · Land use · Urban vegetation · High spatial resolution remote sensing · Light use efficiency

Introduction

Gross primary productivity (GPP) is the sum of photosynthesis at the ecosystem scale (Chapin et al. 2002). It describes the initial inputs of atmospheric carbon to ecosystems and is an important metric of ecosystem function (Heinsch et al. 2006). Models of GPP from satellite remote sensing have been used to estimate carbon uptake at regional-to-global scales, improving constraints on ecophysiological models across many biomes (Ogutu and Dash 2013). However, urban areas are not usually included in such large-scale models due to the small percentage of the global land area covered by cities relative to the major natural biomes and due to the fine-scale spatial heterogeneity of urban areas.

More than half of the global human population now lives in urban areas, and this proportion is expected to grow through the twenty-first century (Grimm et al. 2008). Urbanization replaces native vegetation, often negatively affecting terrestrial carbon storage initially (Seto et al. 2012). In general, urban development reduces primary production in densely vegetated regions (Imhoff et al. 2004), but it can increase primary production in some areas previously covered by agriculture (Zhao et al. 2007) or deserts (Buyantuyev and Wu 2009). Once established, urban vegetation can provide ecosystem services such as local cooling (Oke 1989) and absorption of airborne pollutants (Nowak et al. 2006). Urban vegetation has direct effects on the carbon budget through CO_2 uptake and storage, and through CO_2 release from plant respiration. Urban vegetation has indirect effects on the carbon budget through reduced building energy consumption due to tree shading and windbreaks, modifying soil respiration, and potential CO_2 emissions as energy is used for landscape maintenance

✉ David L. Miller
dlm@geog.ucsb.edu

[1] Department of Geography, University of California, Santa Barbara, 1832 Ellison Hall, Santa Barbara, CA 93106, USA

[2] Department of Environmental Science, Policy, and Management, University of California, Berkeley, 130 Mulford Hall #3114, Berkeley, CA 94720, USA

[3] Minnesota Department of Natural Resources, 500 Lafayette Rd, St. Paul, MN 55155, USA

(Pataki et al. 2006). In this context, there is a need for mapping GPP within urban areas because it is relatively unknown how GPP varies among vegetation and land-use types in cities.

One of the most established methods to calculate GPP from remote sensing is the light use efficiency (LUE) approach, first proposed by Monteith (1972), which assumes that vegetation takes up carbon at a rate relative to incident photosynthetically active radiation (PAR). In this approach, GPP can be calculated on a per-pixel basis as:

$$GPP = FPAR \times PAR \times LUE \quad (1)$$

where GPP is the mass of carbon taken up per unit time (g C m^{-2} d^{-1}), PAR is the incident photosynthetically active radiation per unit time (e.g., MJ m^{-2} d^{-1}), FPAR is the unitless fraction of PAR absorbed by the vegetated surface, and LUE is the conversion rate from absorbed PAR to plant carbon uptake (e.g., g C MJ^{-1}) (Hilker et al. 2008). Versions of this method have been used to estimate large-scale dynamics of GPP in light use (or production) efficiency models, and in situ carbon flux measurements are used both to parameterize and to validate such models at the ecosystem scale (Hilker et al. 2008; Ogutu and Dash 2013). FPAR is often estimated through spectral vegetation indices and radiative transfer modeling (Hilker et al. 2008; Song et al. 2013). LUE has been shown to vary by species and the environmental conditions affecting an individual plant or leaf (e.g., Ahl et al. 2004), but has been successfully modeled by vegetation biome at a variety of scales (Song et al. 2013).

Generally in LUE models each image pixel is labeled as a unique vegetation class due to differences in physiological and functional characteristics among vegetation types (Song et al. 2013). Labeling is a challenge in urban areas because the remote sensing systems used to estimate GPP at regional and global scales (e.g., Landsat TM and MODIS) have spatial resolutions that are too coarse to distinguish small vegetation patches, such as street trees, from urban structures, such as roads and buildings (Raciti et al. 2014). Imagery from such sensors in urban areas is dominated by mixed pixels comprising multiple constructed and vegetated surfaces that each affect FPAR differently. This causes two problems in the context of production efficiency modeling of urban GPP from remote sensing. First, it is difficult to identify unique vegetation types, each of which has different LUE parameters. Second, it is difficult to obtain accurate estimates of FPAR due to the mixing of spectral reflectance characteristics of different vegetated and non-vegetated surfaces within an image pixel.

High spatial resolution imagery has the potential to improve spatial estimates of urban GPP by enhancing detail in classification and vegetation function at finer scales. As urban areas have highly variable surface cover over relatively short distances (Cadenasso et al. 2007), urban land cover classification from remote sensing is often approached using imagery either with high spectral resolution (e.g., Herold et al. 2004; Wetherley et al. 2017) or with high spatial resolution using pixel- or object-based techniques (e.g., Myeong et al. 2001; Myint et al. 2011). While it can be difficult to separate trees from grasses due to their spectral similarity using only multispectral data (e.g., Myeong et al. 2001), additional data sets such as LiDAR (light detection and ranging) can be used to help distinguish vegetation types by height (e.g., Raciti et al. 2014; Alonzo et al. 2016; Hedblom et al. 2017).

In urban GPP studies, the issue of fine-scale surface heterogeneity has been approached by assigning per-pixel estimates of fractional cover (e.g., Zhao et al. 2007; Zhao et al. 2012), considering urban areas as a single vegetation type (such as savanna) in which condition varies as a function of a spectral vegetation index (e.g., Milesi et al. 2003), or by using relatively high spatial resolution imagery to better separate vegetated and non-vegetated surfaces (e.g., As-syakur et al. 2010; Wu and Bauer 2012). More recent research has estimated urban biogenic fluxes as they vary with impervious surface cover, the urban heat island, and plant phenology (Hardiman et al. 2017). Variability of urban primary production by land cover type is often analyzed using large pixels due to data availability and scale (e.g., Imhoff et al. 2004; Zhao et al. 2007).

Urban GPP estimates have often relied on LUE parameters from natural ecosystems (e.g., Zhao et al. 2007) because there have been few field measurements of LUE in cities (e.g., Wu and Bauer 2012). While LUE values have been analyzed extensively within and among natural ecosystems (Hilker et al. 2008), the values have not been evaluated for application to urban vegetation, and few studies locally estimate their LUE parameters (e.g., Wu and Bauer 2012). Therefore, it remains unclear how different vegetation and land-use types individually affect GPP within urbanized areas at a scale in which lawns, trees, and roads can be identified. In general, the importance of unique LUE parameterization of urban vegetation cover types to accurately characterize urban GPP is relatively unknown.

We used high spatial resolution surface reflectance data from WorldView-2 (WV-2) satellite imagery to estimate GPP across the Minneapolis-Saint Paul, Minnesota metropolitan area. We produced a land cover classification using WV-2 imagery, canopy height data from airborne LiDAR, leaf-off color-infrared aerial orthophotos, and regional GIS layers to mask specific land cover/land-use types. We calculated empirical LUE estimates for deciduous broadleaf trees, evergreen needleleaf trees, turf grass, and golf course grass from WV-2 reflectance by using in situ observations of GPP from tree sap flow and eddy covariance flux measurements over a turf grass lawn. We compared our mapped GPP estimates using eddy covariance observations at a height of 40 m from a tall tower (KUOM) near our in situ training sites, and we assessed the variability of GPP by vegetation and land-use type across the

study area. Our research questions were: (1) what is the magnitude and variability of GPP within dominant urban vegetation types, specifically deciduous broadleaf trees, evergreen needleleaf trees, turf grass, and golf course grass; (2) what determines the magnitude and variability of GPP within the major urban land-use types; and (3) how does GPP for urban vegetation compare to natural vegetation?

Methods

Study area

Our study site was a large part (894 km^2) of the Minneapolis-Saint Paul, Minnesota (44° 59' N, 93° 11' W) metropolitan region. The region has a humid continental climate (Köppen Dfa) with warm summers and very cold winters, and receives precipitation year-round. The region has a mean annual temperature of 7.4 °C and mean annual precipitation of 747 mm (Peters et al. 2011). It has two densely developed urban cores ~14 km apart surrounded by extensive suburban residential development. Much of the study area is likely to be influenced by the urban heat island effect (Winkler et al. 1981; Todhunter 1996; Sen Roy and Yuan 2009). The region has been undergoing urban growth and expansion over recent decades (Yuan et al. 2005), and is expected to grow by over 800,000 people between 2010 and 2040 (Metropolitan Council 2015).

We selected this region due to the availability of in situ observations of GPP from sap flux, leaf-level gas exchange, and eddy covariance for dominant urban vegetation types in the region: deciduous broadleaf trees, evergreen needleleaf trees, and turf grass. Common deciduous broadleaf trees included ash (*Fraxinus* spp.), elm (*Ulmus* spp.), red oak (*Quercus rubra*), eastern black walnut (*Juglans nigra*), and American basswood (*Tilia americana*); common evergreen needleleaf trees included spruce (*Picea* spp.) and pine (*Pinus* spp.) species (Peters and McFadden 2012); and common turf grass species included Kentucky bluegrass (*Poa pratensis*), tall fescue (*Festuca arundinacea*), and perennial ryegrass (*Lolium perenne*) (Hiller et al. 2011). We used additional eddy covariance measurements acquired at 40 m height on a tall radio tower (KUOM) near the in situ flux observations of tree and turf grass to compare with our mapped GPP (Peters and McFadden 2012; Menzer et al. 2015; Menzer and McFadden 2017).

Land cover classification and validation

The 2 m resolution WorldView-2 imagery was acquired on July 17 and July 28, 2010, and was orthorectified (NAD83, UTM Zone 15 N) to a digital surface model (DSM) gridded at 1 m spatial resolution (Potapenko 2014). The DSM was derived from a multi-return LiDAR point cloud acquired during flights in 2011 and 2012 at 1.5 points m^{-2} by a Leica ALS50-II MPiA sensor and at either 2 or 8 points m^{-2} using a FLI-MAP sensor (Fugro Horizons, Inc. and the Minnesota Department of Natural Resources 2012). We atmospherically corrected the WV-2 imagery with the FLAASH module in ENVI version 5.1 (Adler-Golden et al. 1998) and mosaicked the WV-2 images. Then we resampled the 2 m mosaic to 1 m spatial resolution using a nearest neighbor approach to match the DSM and its associated canopy height model, verified its alignment with the DSM base map (RMSE = 1.69 m, SD = 0.79 m), and clipped the data to the final extent of the total study area.

We classified land cover/land-use using a hierarchical approach. We first computed the Normalized Difference Vegetation Index (NDVI = (NIR − red) / (NIR + red); Tucker 1979). We corrected a small difference in NDVI between the two WV-2 images using a linear regression (Eq. 2) from polygons sampled within a 33 km^2 overlapping region of the two images.

$$NDVI_{July\ 28} = 1.0246 \times NDVI_{July\ 17} + 0.0040, \quad (2)$$

$$R^2 = 0.9869, p < 0.001$$

Then, we used a maximum likelihood supervised classification (Jia and Richards 1994) including all WV-2 bands and the NDVI to distinguish between vegetated and non-vegetated pixels. Water was masked using a modified version of an open water features GIS layer (Metropolitan Council 2013) to avoid confusion with shadows and vegetation.

Trees and turf grasses were separated using a 1 m height threshold, following Raciti et al. (2014), using a canopy height model gridded from the DSM's LiDAR point cloud. Gaps in the model were mitigated using a 3 × 3 m mean filter. We relabeled prominent areas of electric transmission lines that had been misclassified as trees to be turf grass. We separated turf grass within golf courses (referred to as golf course grass) from all other grass surfaces (referred to as turf grass) using a GIS layer of land-use types (Metropolitan Council 2011). Although they are of the same plant functional type, golf courses have a different species composition and they receive higher levels of maintenance and nutrient and water inputs as compared to other turf grass sites (Qian and Follett 2002). Deciduous broadleaf and evergreen needleleaf trees were separated by thresholding a ratio of the WV-2 NDVI and the NDVI from digital color-infrared orthophotos acquired during leaf-off conditions in April 2010 at 0.3 m resolution (Minnesota Department of Natural Resources and Surdex Corporation 2010), and smoothed using a 5 × 5 m median filter in the tree classes.

Other classes were created to exclude them from GPP calculation due to our focus on common urban land covers. Wetlands have different physiological characteristics from our vegetation classes (Chapin et al. 2002) and we did not have in situ observations of wetland GPP. They were labeled

using a modified GIS layer of wetlands and wet areas (Metropolitan Mosquito Control District 2012) and replaced turf grass, golf course grass, and impervious and soil pixels within the layer's extent, not including well-drained grasses and woodlands. Agriculture was labeled using a modified GIS layer of land-use types (Metropolitan Council 2011). Clouds were masked using manually drawn polygons.

We assessed the accuracy of our land cover classification for the built-up and urban vegetation classes, namely deciduous broadleaf trees, evergreen needleleaf trees, turf grass, golf course grass, and impervious and soil. For accuracy assessment, turf grass and golf course grass were combined because these were distinguished using a land-use map in a GIS rather than from raster imagery. We randomly sampled 100 initial single-pixel targets for each land cover class, and we assessed each target using the WV-2 imagery, a ~0.3 m (1 ft) spatial resolution RGB USGS orthophoto acquired in early spring 2012, and imagery from Google Earth. We excluded any targets that could not be unambiguously labeled using the available validation imagery, resulting in 275 evaluated targets.

NDVI and FPAR

We calculated FPAR from the NDVI following Sims et al. (2006) as:

$$FPAR = 1.24 \times NDVI - 0.168 \quad (3)$$

The relationship was based on ground measurements of multiple plant functional types and is similar to other published NDVI-FPAR linear relationships (Ruimy et al. 1994; Song et al. 2013). Few NDVI-FPAR equations have been published specifically for urban vegetation types, but Eq. 3 was similar to a relationship for turf grass from Wu and Bauer (2012; FPAR = 1.29 × NDVI – 0.29). In this study, we used the relationship from Sims et al. (2006) for our entire study region to maintain a consistent NDVI-FPAR relationship across vegetation types. Eq. 3 has been applied using MODIS NDVI in light use efficiency studies (e.g., Wu et al. 2012), and we converted our WV-2 NDVI to approximate MODIS NDVI to account for differences in the sensors' spectral bands. Similar NDVI conversions have been implemented in other urban GPP studies (e.g., Zhao et al. 2007). We developed an empirical WV-2 NDVI to MODIS NDVI linear regression by spectrally resampling an Airborne Visible/Infrared Imaging Spectrometer (AVIRIS; Green et al. 1998) image from July 29, 2009 of Rosemount, Minnesota to approximate the WV-2 and MODIS spectral bands using spectral response functions in ENVI. We atmospherically corrected the AVIRIS radiance image with ACORN 6.080101 mode 1.5 using a summer atmospheric model, derived water vapor at 940 nm, and 50 km image atmosphere visibility (ImSpec LLC – Palmdale, CA, USA). We used every available pixel in the AVIRIS image extent. Pixels below the line of Eq. 4 were water bodies in nearly all cases.

$$NDVI_{MODIS} = 1.01 \times NDVI_{WV-2} + 0.025 \quad (4)$$

We masked all pixels below this line and regressed the remaining pixels, generating Eq. 5.

$$NDVI_{MODIS} = 0.9842 \times NDVI_{WV-2} + 0.01039, \quad (5)$$

$$R^2 = 0.9994, p < 0.001$$

We applied Eq. 5 to the WV-2 NDVI, and then used Eq. 3 to produce an FPAR image.

In situ CO_2 flux data

We used in situ observations of tree and turf grass GPP and PAR in a first-ring suburban neighborhood in the center of our study area to derive an empirical LUE estimate for each vegetation type.

For trees, we used GPP estimates based on sap flow and leaf-level gas exchange measurements on seven genera representing evergreen needleleaf and deciduous broadleaf tree plant functional types (Peters and McFadden 2012). These data were collected in 2007 and 2008 on representative trees growing in park-like conditions at four locations in the Minneapolis-Saint Paul metropolitan area. Maintenance was considered to be low at all sites, with no irrigation, little or no fertilizer, and regular mowing. Canopy-level meteorological measurements were used to convert whole-tree transpiration rates obtained from sap flow measurements to canopy conductance estimates. Leaf-level gas exchange measurements of photosynthesis and stomatal conductance were used to convert canopy conductance to continuous estimates of canopy photosynthesis (i.e., tree GPP). We averaged across genera to derive separate GPP estimates for deciduous broadleaf trees and evergreen needleleaf trees.

For turf grass, we used GPP estimates from eddy covariance CO_2 flux measurements that were acquired during 2005–2009 at a 1.5 ha turf grass field, also in a first-ring suburban location (Hiller et al. 2011). The field was representative of low-maintenance lawns, with regular mowing, no clipping removal, no irrigation, and one application of fertilizer per year (Hiller et al. 2011). Turf grass net ecosystem exchange (NEE) was measured directly by the eddy covariance system, and GPP was calculated by estimating ecosystem respiration based on the temperature response of the CO_2 flux during nighttime, and then subtracting it from NEE. We used only observed (i.e., not gap-filled) data from the turf grass eddy covariance site.

We did not have in situ measurements for golf course grass. However, Peters and McFadden (2012) modeled GPP for irrigated grass based on measurements at the turf grass site when water was not limiting growth in the spring and fall.

Irrigated grass GPP during midsummer was estimated by fitting these data to light-response curves and ecosystem respiration models using midsummer soil temperature and soil radiation data. For golf course grass, we used this modeled GPP. It may underestimate actual golf course grass GPP because it does not account for fertilization or other benefits of increased maintenance.

We made an independent assessment of our mapped GPP estimates using eddy covariance CO_2 flux measurements from a height of 40 m on a tall tower near the turf grass and tree sites (Peters and McFadden 2012; Menzer et al. 2015; Menzer and McFadden 2017). The reference GPP was obtained by applying the flux partitioning algorithm by Reichstein et al. (2005) to the biogenic fraction of the net CO_2 flux measurements (Menzer and McFadden 2017). We used half-hourly flux observations, and filtered the data according to the following criteria: (1) the measurement was from the northwest wind sector (270–360°) over the predominant residential land-use type; (2) the measurement was observed, rather than gap-filled; and (3) the cumulative flux source was >99% within the residential land-use type (Menzer and McFadden 2017).

LUE and GPP estimation

In situ observations at half-hourly intervals were used to generate characteristic mean diurnal cycles of midsummer daily GPP and PAR for the plant functional types of interest and the tall tower (e.g., Soegaard and Møller-Jensen 2003). The turf grass site had available summertime eddy covariance data from 2006 to 2008, but we omitted data from 2007 because conditions during the midsummer period were hot and dry compared to long-term averages (1981–2010, National Climatic Data Center). The tree sap flow and tall tower eddy covariance data were only available in 2008 for the time window near our image acquisition. We estimated PAR from incident shortwave radiation (W m^{-2}) measurements at the turf grass site multiplied by 0.45 (Running and Zhao 2015). Only daylight (PAR > 0.45 W m^{-2}) observations of GPP were used and we removed values due to rainy or cloudy conditions or instrument error. We averaged GPP and PAR at half-hourly time points, and summed the average values to produce composite diurnal estimates of GPP (g C m^{-2} d^{-1}) and incident PAR (MJ m^{-2} d^{-1}) over a 4-week interval surrounding our July image acquisition date. We also tested 2- and 3-week averaging intervals, but the composite sums of GPP and PAR were relatively insensitive to the range used. We selected the 4-week interval because of the greater number of data points.

To estimate LUE, we extracted FPAR estimates for deciduous broadleaf trees, evergreen needleleaf trees, and turf grass. We used manually delineated polygons containing only the tree or turf grass areas where GPP was measured in situ. At the sites used to train the LUE values, deciduous broadleaf trees had a mean FPAR (± SD) of 0.88 ± 0.04, evergreen needleleaf trees had a mean FPAR of 0.83 ± 0.07, and turf grass had a mean FPAR of 0.74 ± 0.03. To parameterize golf course grass FPAR, we used its mean FPAR value for the total study area because the golf course grass GPP values were modeled rather than measured at a field site. The empirical LUE estimates were calculated using the site polygons' FPAR and the vegetation types' 4-week GPP and PAR values.

We generated our composite map of GPP for clear-sky, midsummer conditions by multiplying the WV-2 FPAR raster by the 4-week PAR based on the 40 m tower observations (12.09 MJ m^{-2} d^{-1}) and the LUE estimates by mapped vegetation type from the land cover classification.

GPP validation and variability

We used flux footprints from the 40 m tower site to compare with our GPP map. Each footprint represented the modeled ground area from which 80% of a given flux measurement originated (Kljun et al. 2004). We created a composite footprint for the tall tower flux observations by merging the footprints corresponding to the half-hourly flux observations used to construct the 4-week mean diurnal cycle. We extracted the GPP estimates of all vegetated pixels within the merged footprint and used the mean value to independently compare with the tall tower's summed mean diurnal cycle.

We quantified variation in urban GPP by analyzing how GPP varied among and within dominant vegetation and land-use types. Land-use types were derived from the Generalized Land Use 2010 GIS layer (Metropolitan Council 2011) and included: airport; golf course; industrial; institutional; major highway; mixed use; office; park, recreational, or preserve; residential; retail; and undeveloped.

Results

Vegetation classification

Our land cover classification (Fig. 1) had an overall accuracy of 80% (kappa = 0.74) for built-up and vegetated urban land cover classes, which included impervious and soil, deciduous broadleaf tree, evergreen needleleaf tree, and grass (turf grass and golf course grass combined) classes (Table 1). We did not include water, wetland, agriculture, or clouds in the accuracy assessment because those classes were not the focus of our urban GPP analysis and they were mapped primarily from existing GIS data sources rather than our imagery. Grouping the vegetation classes together, we had an overall accuracy of 98% (kappa = 0.95) in classifying vegetated areas versus impervious and soil. The tree classes combined were separable from the grass class with an overall accuracy of 94% (kappa = 0.85), and the accuracy was 74% (kappa = 0.62) in distinguishing among the vegetation classes.

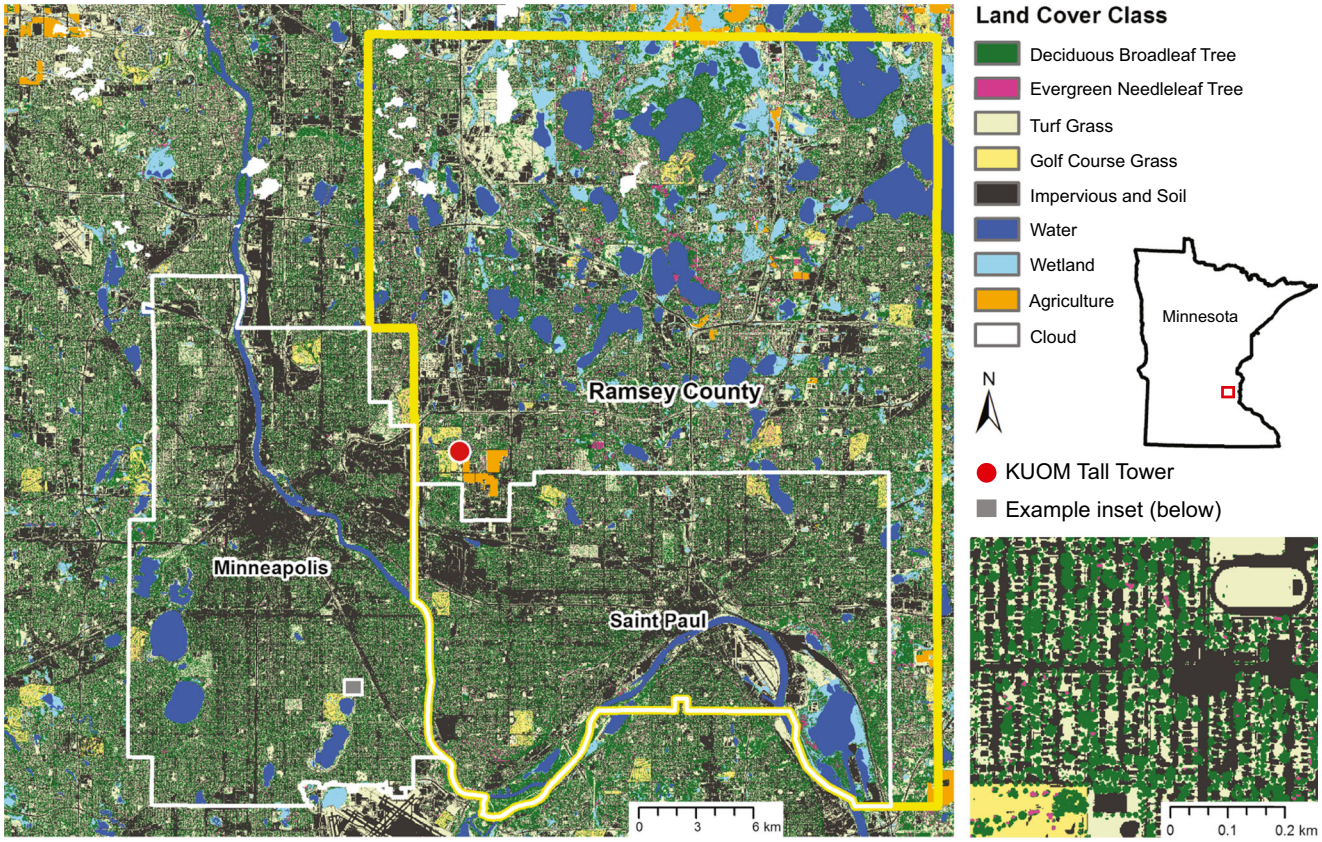

Fig. 1 Land cover classification for the full study extent (32 × 28 km) (left), with the KUOM flux tower location indicated by a red circle, the Minneapolis and Saint Paul boundaries by the white lines, and the Ramsey County boundary by the yellow lines. Inset (lower right) location indicated by gray box. Location of study area in Minnesota indicated by red box in state outline (right)

The greatest misclassification was between the deciduous broadleaf and evergreen needleleaf tree classes. Nearly all real evergreen needleleaf trees were correctly mapped (Producer's accuracy = 0.92), but many trees mapped as evergreen needleleaf were actually deciduous broadleaf (User's accuracy = 0.47). Given the leaf-off imagery we had available, we believed it was more important to accurately map every real evergreen needleleaf tree due to the very small area of evergreen needleleaf trees in the image. As a consequence, we misclassified a small amount of the dominant deciduous broadleaf tree class as evergreen needleleaf trees. We also had misclassification between deciduous broadleaf trees and grass. Seven pixel targets were classified as turf grass but were deciduous broadleaf trees, mostly at the edge of a tree canopy, in canopy gaps, or consisted of shrubs. This is likely partially a result of the low pass filter we used to reduce pits and gaps in the canopy height model.

FPAR retrieval

The distributions of FPAR by vegetation type are shown in Fig. 2. Deciduous broadleaf trees, evergreen needleleaf trees, and golf course grass had similarly high FPAR values, while the turf grass had a broader distribution with a lower mean value. The mean FPAR (± SD) values were 0.87 ± 0.09 for deciduous broadleaf trees, 0.86 ± 0.08 for evergreen needleleaf trees, 0.76 ± 0.13 for turf grass, and 0.85 ± 0.09 for golf course grass, all with left-skewed distributions.

Mean diurnal cycles and LUE

The mean diurnal cycles from the in situ observations are shown in Fig. 3. The deciduous broadleaf and evergreen needleleaf tree GPP exhibited a rapid increase in the morning and slow decline in the afternoon. Deciduous broadleaf trees had a lower daily maximum GPP than did evergreen needleleaf trees. The turf grass GPP reached a daily maximum in mid-morning that remained relatively constant until late afternoon, while the modeled golf course grass GPP reached higher values in a parabolic fashion. The GPP data at the 40 m KUOM flux tower were similar to the turf site, but had a higher constant daily maximum closer to noon.

Golf course grass had the highest GPP, followed by turf grass, evergreen needleleaf trees, and deciduous broadleaf trees (Table 2). The incident PAR observations were nearly the same across all time periods with values ~12 MJ m^{-2} d^{-1}.

Table 1 Accuracy assessment table for built-up and vegetated urban land cover. Overall accuracy was 80% (kappa = 0.74). Golf and turf grass were considered as one class for accuracy assessment because they were distinguished from one another using a GIS layer rather than the raster image classification

		Reference					
		Deciduous Broadleaf Tree	Evergreen Needleleaf Tree	Grass (Turf + Golf)	Impervious and Soil	Total	User's Acc.
Classification	Deciduous Broadleaf Tree	54	3	2	0	59	0.92
	Evergreen Needleleaf Tree	33	33	3	1	70	0.47
	Grass (Turf + Golf)	7	0	52	3	62	0.84
	Impervious and Soil	0	0	2	82	84	0.98
	Total	94	36	59	86	275	
	Producer's Acc.	0.57	0.92	0.88	0.95		

We found that LUE was lowest for deciduous broadleaf trees (0.24 g C MJ^{-1}) and highest for golf course grass (1.14 g C MJ^{-1}), with evergreen needleleaf trees (0.56 g C MJ^{-1}) and turf grass (0.66 g C MJ^{-1}) in between.

Comparison to tall tower flux measurements

The sum of the mean diurnal cycle of GPP measured at the 40 m tower during the 4-week time period was 8.01 g C m^{-2} d^{-1}, while the corresponding sum of PAR was 12.09 MJ m^{-2} d^{-1}. The union of the 80% contribution flux footprint polygons from the 40 m tower (Fig. 4) was used to spatially aggregate our mapped GPP estimates. Our GPP map had a mean value of 7.10 g C m^{-2} d^{-1} (area weighted mean SD = 0.67 g C m^{-2} d^{-1}) for the parameterized vegetation classes within the 40 m tower footprint area. We considered our GPP map's estimate, 11.4% lower than the tower GPP, to be reasonable given the inherent variability in both our model and the tower data.

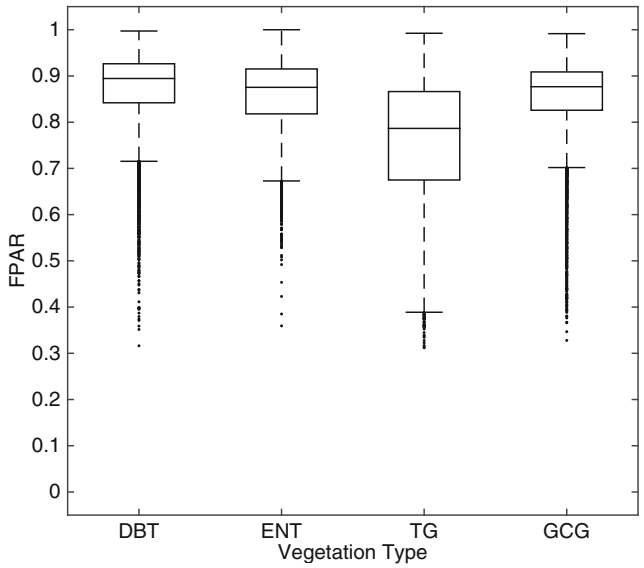

Fig. 2 Box plots of FPAR for deciduous broadleaf tree (DBT), evergreen needleleaf tree (ENT), turf grass (TG), and golf course grass (GCG) for the full study extent (10,000 samples per class). The middle line of the box is the median, the outer edges of the box are the 25th and 75th percentiles, and dashed lines are whiskers that extend to 1.5 × the standard deviation, with values greater than this from the median shown as dots

GPP totals

The majority of our map's vegetated areas were deciduous broadleaf trees and turf grass, with only small areas of evergreen needleleaf trees and golf course grass (Table 3). The vegetation cover of the total study area was 52.1% including all land cover classes. We found consistent percent cover for each mapped vegetation type among the administrative boundaries of Minneapolis, Saint Paul, and Ramsey County. However, the percent impervious and soil cover was greater in the major cities of Minneapolis and Saint Paul than in Ramsey County and the total study area.

For the total study area, the mean GPP across the parameterized vegetation classes and the impervious and soil class was 2.64 g C m^{-2} d^{-1}, and was 4.45 g C m^{-2} d^{-1} within the vegetated areas. The mean estimates of GPP were consistent in the vegetated classes. For the total study area, deciduous broadleaf trees had the lowest mean GPP (2.52 g C m^{-2} d^{-1}), evergreen needleleaf trees (5.81 g C m^{-2} d^{-1}) and turf grass (6.05 g C m^{-2} d^{-1}) had similar means, and golf course grass (11.77 g C m^{-2} d^{-1}) had the highest mean GPP. The percent contributions to total GPP by vegetation class were similar across the selected regions, with turf grass contributing 55–62% and deciduous broadleaf trees contributing 27–32% of the total GPP. Both classes had similar total areas, but the lower LUE of the deciduous broadleaf trees resulted in lower GPP contributions. Evergreen needleleaf trees and golf course grass had small areas and little impact on the GPP totals.

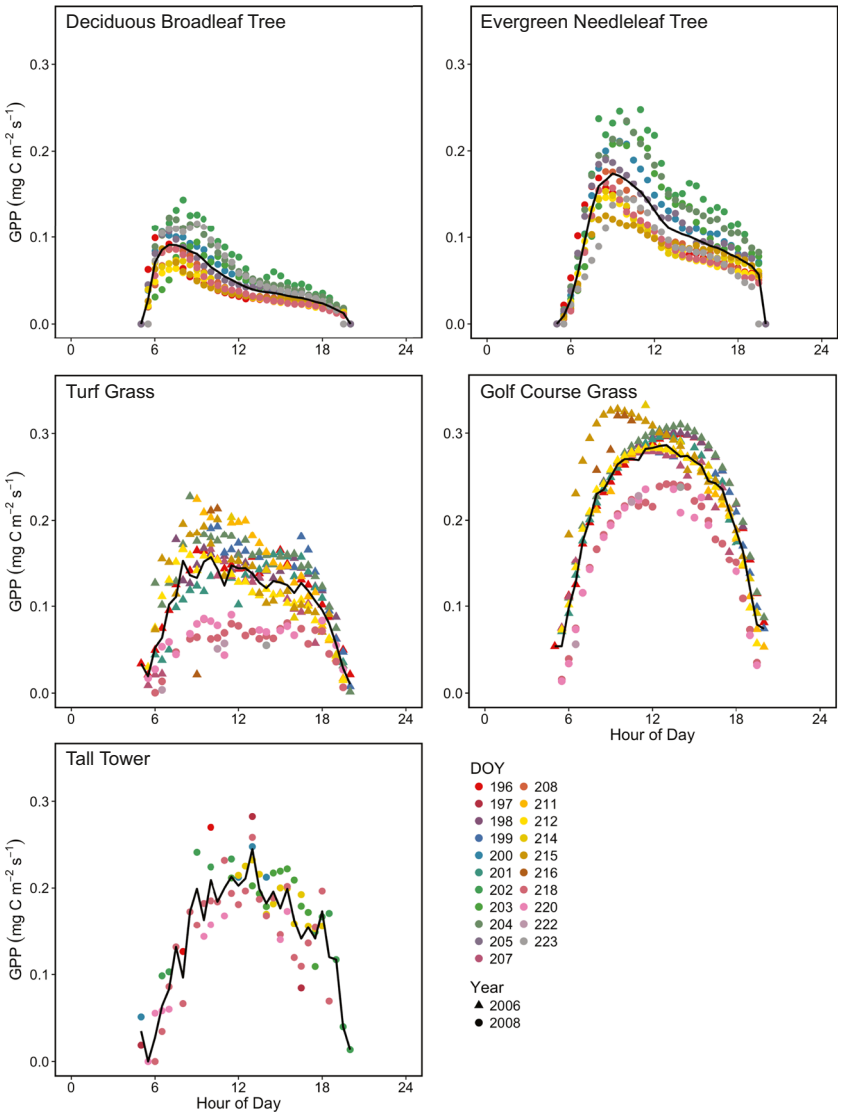

Fig. 3 In situ flux observations used to calculate mean daily sums of GPP and PAR during 4-week interval. Mean values at half-hourly intervals are black lines, colors are day of year (DOY), triangles represent 2006 and circles 2008. The deciduous broadleaf and evergreen needleleaf tree GPP data were from sap flow measurements in 2008. The turf grass GPP data were from eddy covariance measurements in 2006 and 2008. The golf course grass GPP data were modeled based on turf grass eddy covariance measurements under peak growing conditions in 2006 and 2008. The tall tower eddy covariance data were from 2008. All data are during daylight (PAR > 0.45 W m^{-2})

Variability of GPP among and within vegetation types

The coefficients of variation (CV = SD / mean) of GPP were 0.10 for deciduous broadleaf trees, 0.09 for evergreen needleleaf trees, 0.18 for turf grass, and 0.10 for golf course grass. The CV of GPP for turf grass was nearly twice as large as those for the other vegetation classes, and all the distributions were left-skewed (Fig. 5). Deciduous broadleaf trees had a more peaked distribution but had a similar CV to evergreen needleleaf trees and golf course grass due to their lower mean GPP.

Table 2 Parameters from sums of mean diurnal cycles and site polygons in FPAR image to estimate LUE: GPP (g C m^{-2} d^{-1}), FPAR (unitless), PAR (MJ m^{-2} d^{-1}), and LUE (g C MJ^{-1} PAR)

	GPP	FPAR	PAR	LUE
Deciduous Broadleaf Tree	2.54	0.88	12.08	0.24
Evergreen Needleleaf Tree	5.57	0.83	12.08	0.56
Turf Grass	5.96	0.74	12.15	0.66
Golf Course Grass	11.79	0.85	12.11	1.14

GPP among and within land-use types

The major urban land-use types varied widely in percent cover of the different vegetation classes (Table 4). We calculated percent cover using only the vegetation classes and the impervious and soil class. We did not include the other land cover classes (water, wetlands, agriculture, and clouds) in our percent cover calculations because those classes are not typical urban land cover classes that were the focus of our GPP analysis.

Residential areas had 63.2% vegetation cover, with a higher percent cover of deciduous broadleaf trees (34.9%) than all other land-use types except parks, recreational areas,

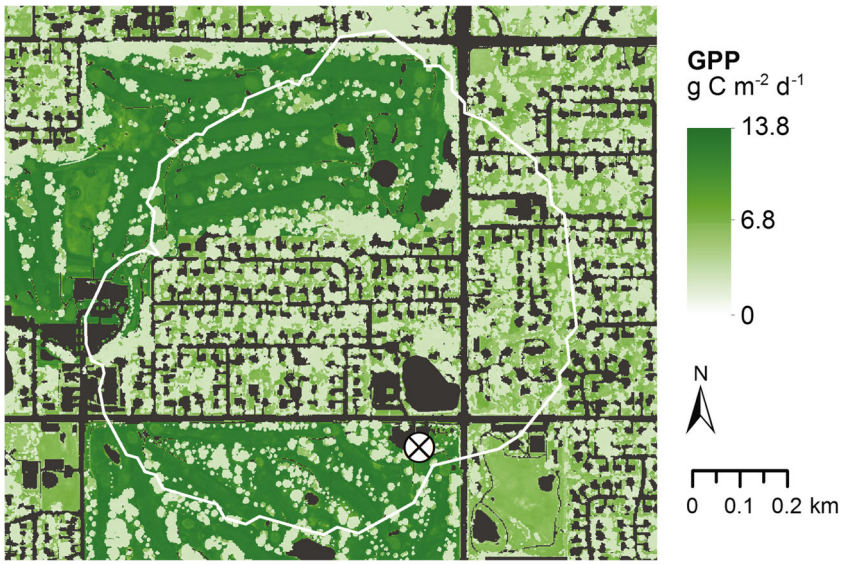

Fig. 4 Union of high quality 80% contribution polygons forming tall tower ground footprint (white boundary, tower is '×') during 4-week interval over a clipped out area of the GPP map. Non-vegetated areas are shown in black

or preserves and undeveloped areas, but a similar percent cover of turf grass (24.9%) compared to the other land-use types. Deciduous broadleaf trees had less than 10% cover in the most built-up land-use categories such as industrial, mixed use, retail, and airport, but had high percent cover in less developed land-use types such as the undeveloped and park, recreational, or preserve classes. Evergreen needleleaf trees had low percent cover across all land-use categories because they are less commonly planted in the region. Turf grass had 26.1% cover for the total study area, and had the highest percent cover at 48.5% for the airport land-use type, while golf courses had 65.3% grass cover and a total of 91.1% vegetation cover, the highest of any land-use type. In general, land-use types with 30–60% vegetation cover had greater turf grass cover than deciduous broadleaf tree cover, and only at low levels of vegetation cover (<30%) was turf grass cover also strongly reduced (Fig. 6).

When expressed per unit of land area (i.e., including impervious surfaces and soil), we observed large differences in mean GPP among land-use types, but when compared per unit vegetated area, the mean land-use GPP values exhibited low variability (Table 5). The overall differences in land-use GPP were mostly attributable to the percent vegetation cover. Turf grass accounted for the majority (59.0–94.8%) of the total GPP within every land-use type (excluding golf courses) (Table 6). Turf grass GPP had a larger CV across the land-use types (0.16 to 0.21) than either of the tree classes or the golf course grass. The CV for golf course grass GPP (0.10) was similar to the tree classes rather than the turf grass. Among all land-use types, the CV for deciduous broadleaf trees ranged from 0.07 to 0.14 and the CV for evergreen needleleaf trees ranged from 0.07 to 0.11. Land-use types with more impervious and soil cover generally had greater CVs.

The mean GPP values of the land-use types had a strong linear relationship ($y = 0.04x + 0.21$, $R^2 = 0.98$, $p < 0.001$) with percent vegetation cover, not including golf courses (Fig. 7a). Golf courses had the highest percent vegetation cover, and the uniquely high LUE parameterization for golf course grass resulted in a mean GPP twice as large as the value predicted by the other land-use types' linear trend. Mean vegetation GPP (including deciduous broadleaf trees, evergreen needleleaf trees, and turf grass combined) did not exhibit strong variability by land-use type, also excluding golf courses ($y = -0.06x + 4.92$, $R^2 = 0.21$, $p = 0.19$; Fig. 7b).

Discussion

Evaluation of GPP parameters

Vegetation cover and GPP totals

The percent vegetation cover of the total study area (52.1%) was similar to vegetated, suburban sites in Montreal, Canada (50%) (Bergeron and Strachan 2011), Helsinki, Finland (44%) (Järvi et al. 2012), Syracuse, New York (48.2%) (Myeong et al. 2001), and a park site in Essen, Germany (52%) (Kordowski and Kuttler 2010). The tree canopy cover was 28.0% for the total study area, similar to high spatial resolution imagery studies in Boston, Massachusetts (25.5%) (Raciti et al. 2014), Santa Barbara, California (25.4%) (Alonzo et al. 2016), Syracuse, New York (26.6%) (Myeong et al. 2001), Leipzig, Germany (19%) (Strohbach and Haase 2012), and Berlin, Germany (30.4%) (Tigges et al. 2017). Turf grass cover (22.9%) was similar to estimates of residential areas in

Table 3 Summary of vegetation classes and GPP within the full extent of the study area, the cities of Minneapolis and Saint Paul, and Ramsey County. (**a**) Total area (km^2); (**b**) Mean GPP (± SD; g C m^{-2} d^{-1}); (**c**) Total daily GPP (± SD; Mg C d^{-1}); and (**d**) Percent contribution to total daily GPP (± SD) by vegetation type

a. Areas (km^2)	Full Study Extent	Minneapolis	Saint Paul	Ramsey County
Deciduous Broadleaf Tree	228.1	35.3	38.0	115.9
Evergreen Needleleaf Tree	22.3	2.1	3.3	13.5
Turf Grass	204.4	30.0	28.0	95.8
Golf Course Grass	11.1	1.3	1.7	4.9
Impervious and Soil	317.6	70.6	61.9	139.7
Total Vegetated	465.9	68.7	71.1	230.1
Total Area	894.0	148.6	145.0	439.8
b. Mean GPP (g C m^{-2} d^{-1})	Full Study Extent	Minneapolis	Saint Paul	Ramsey County
Deciduous Broadleaf Tree	2.52 ± 0.25	2.45 ± 0.28	2.51 ± 0.27	2.54 ± 0.24
Evergreen Needleleaf Tree	5.81 ± 0.52	5.73 ± 0.54	5.86 ± 0.53	5.81 ± 0.51
Turf Grass	6.05 ± 1.07	5.97 ± 1.06	6.02 ± 1.06	6.10 ± 1.04
Golf Course Grass	11.77 ± 1.20	11.65 ± 1.21	11.80 ± 1.09	11.76 ± 1.18
Total Vegetated	4.45 ± 0.76	4.26 ± 0.76	4.27 ± 0.72	4.41 ± 0.72
Total Vegetated + Impervious and Soil	2.64 ± 0.59	2.10 ± 0.53	2.28 ± 0.53	2.75 ± 0.57
c. Total GPP (Mg C d^{-1})	Full Study Extent	Minneapolis	Saint Paul	Ramsey County
Deciduous Broadleaf Tree	576 ± 57	86 ± 10	95 ± 10	295 ± 28
Evergreen Needleleaf Tree	129 ± 12	12 ± 1	19 ± 2	78 ± 7
Turf Grass	1236 ± 218	179 ± 32	169 ± 30	584 ± 100
Golf Course Grass	131 ± 13	15 ± 2	20 ± 2	58 ± 6
Total	2071 ± 150	292 ± 22	304 ± 20	1015 ± 67
d. GPP	Full Study Extent	Minneapolis	Saint Paul	Ramsey County
Deciduous Broadleaf Tree	27.8 ± 2.8%	29.5 ± 3.4%	31.4 ± 3.4%	29.0 ± 2.8%
Evergreen Needleleaf Tree	6.3 ± 0.6%	4.1 ± 0.4%	6.4 ± 0.6%	7.7 ± 0.7%
Turf Grass	59.7 ± 10.5%	61.2 ± 10.9%	55.5 ± 9.8%	57.6 ± 9.8%
Golf Course Grass	6.3 ± 0.6%	5.1 ± 0.5%	6.7 ± 0.6%	5.7 ± 0.6%

Sacramento, California (24.5%) (Akbari et al. 2003) and several major cities in Sweden (22.5%) (Hedblom et al. 2017).

The midsummer GPP of our total 894 km^2 study area was 2071 Mg C d^{-1} (Table 3c; Table 6). The similar fractional contributions to GPP of the different vegetation types in Minneapolis, Saint Paul, Ramsey County, and the total study area suggest that, at the city or county scale, there were no large differences in vegetation type composition or vegetation condition as evidenced by NDVI-derived FPAR. Turf grass was responsible for more than half of the total GPP for the region due to its large area of coverage (22.9%) and high GPP compared to trees. Deciduous broadleaf trees had the largest area of cover (25.5%) among vegetation classes, but were responsible for only 27 to 32% of the total GPP for the selected regions due to their low GPP (Table 3d). Evergreen needleleaf trees and golf course grass combined never constituted more than 14% of the total GPP due to their small cover fractions.

The 11.4% difference between our mean vegetation GPP mapped within the tower footprint and the GPP calculated from the tall tower CO_2 flux measurements was reasonable given the sources of uncertainty inherent in the two approaches. First, the land cover map is subject to error in land cover classification. Second, there is uncertainty in GPP estimation from the in situ data. For example, the eddy covariance technique has errors associated with bias due to sensor configuration and data processing of typically 5–10% and random error due to atmospheric turbulence of ~5% (Baldocchi 2008). There is also uncertainty in estimating anthropogenic fluxes at an urban site, removing them to determine the vegetation CO_2 fluxes, and modeling GPP with flux partitioning approaches (Menzer and McFadden 2017). The error associated with sap flow and leaf-level gas exchange estimation of tree GPP was assumed to be 29% and 23% for evergreen needleleaf and deciduous broadleaf trees, respectively (Peters and McFadden 2012). The spatial distribution of the flux footprint is also a potential

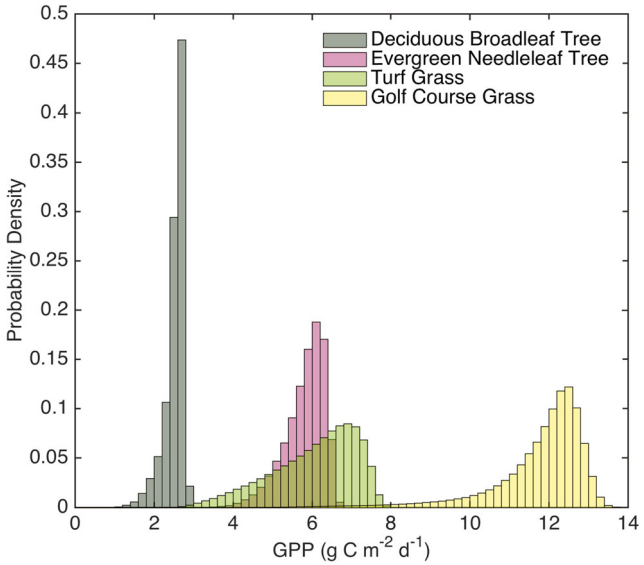

Fig. 5 Normalized histogram of GPP (g C m^{-2} d^{-1}) for each vegetation cover type for the total study area

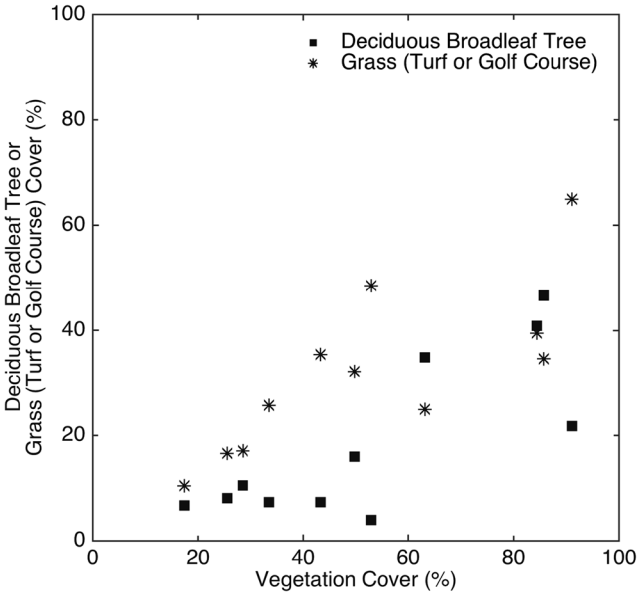

Fig. 6 Vegetation cover (%) plotted against deciduous broadleaf trees or grass (turf or golf course grass) cover (%) within each land use type. See Table 4 for specific land use values

source of uncertainty (Kljun et al. 2004), but this is less severe due to the temporal aggregation of the half-hourly footprints into one cumulative polygon (Menzer and McFadden 2017).

Few published remote sensing studies of urban GPP have reported midsummer (rather than annual) values that are directly comparable to those reported in this study. A study of the Detroit metropolitan region by Zhao et al. (2007) reported summer GPP of ~15 g C m^{-2} d^{-1} compared to our study region mean GPP of 2.64 g C m^{-2} d^{-1}. The difference is partially attributable to the use of LUE parameters based on natural forests, grasslands, and agricultural crops in Zhao et al. (2007), and also attributable to the greater extent of the Detroit study region beyond the city center in Zhao et al. (2007) compared to our study. This could lead to reduced impervious surface cover and greater areas of non-urban tree cover. The leaf area index (LAI) of urban forests can be lower than in natural forests (Peters and McFadden 2010) and above ground biomass for urban trees can be 20% less than trees in natural forests for the same diameters at breast height (Nowak 1994).

FPAR

The FPAR of our turf grass lawn (0.76 ± 0.13) was lower than the more uniformly irrigated and well-maintained golf course grass (0.85 ± 0.09), reflecting differences in species composition and management practices (Qian and Follett 2002) and

Table 4 Percent cover within built-up and urban vegetation areas only, with all non-urban land cover classes removed (water, clouds, wetlands, and agriculture)

	Impervious and Soil	All Vegetation	Deciduous Broadleaf Tree	Evergreen Needleleaf Tree	Turf Grass	Golf Course Grass
Total Study Area	40.5%	59.5%	29.1%	2.8%	26.1%	1.4%
Airport	47.1%	52.9%	3.9%	0.5%	48.5%	0%
Golf Course	8.9%	91.1%	21.8%	4.0%	0%	65.3%
Industrial	74.5%	25.5%	8.1%	0.7%	16.6%	0%
Institutional	50.3%	49.7%	16.0%	1.6%	32.1%	0%
Major Highway	56.7%	43.3%	7.3%	0.5%	35.4%	0%
Mixed Use	66.5%	33.5%	7.3%	0.6%	25.7%	0%
Office	71.5%	28.5%	10.5%	0.8%	17.1%	0%
Park, Rec., or Preserve	14.3%	85.7%	46.7%	4.4%	34.6%	0%
Residential	36.8%	63.2%	34.9%	3.4%	24.9%	0%
Retail	82.6%	17.4%	6.7%	0.4%	10.4%	0%
Undeveloped	15.6%	84.4%	40.9%	4.0%	39.5%	0%

Table 5 Mean GPP (± SD; g C m^{-2} d^{-1}) for the total study area by land use type for different land cover and vegetation type categories

	All Vegetation + Impervious and Soil	All Vegetation	Deciduous Broadleaf Tree	Evergreen Needleleaf Tree	Turf Grass	Golf Course Grass
Total Study Area	2.64	4.45	2.52 ± 0.25	5.81 ± 0.52	6.05 ± 1.07	11.77 ± 1.20
Airport	2.57	4.85	2.58 ± 0.22	6.12 ± 0.41	5.02 ± 1.07	0
Golf Course	8.48	9.31	2.59 ± 0.19	5.89 ± 0.46	0	11.77 ± 1.20
Industrial	1.19	4.68	2.44 ± 0.30	5.77 ± 0.58	5.73 ± 1.13	0
Institutional	2.40	4.82	2.48 ± 0.27	5.64 ± 0.58	5.95 ± 0.98	0
Major Highway	2.17	5.01	2.46 ± 0.29	5.67 ± 0.63	5.52 ± 1.11	0
Mixed Use	1.69	5.04	2.40 ± 0.31	5.58 ± 0.60	5.78 ± 1.00	0
Office	1.32	4.63	2.41 ± 0.30	5.63 ± 0.58	5.94 ± 1.07	0
Park, Rec., or Preserve	3.64	4.25	2.60 ± 0.19	5.98 ± 0.43	6.26 ± 1.02	0
Residential	2.61	4.12	2.50 ± 0.26	5.76 ± 0.53	6.17 ± 1.00	0
Retail	0.76	4.38	2.37 ± 0.32	5.60 ± 0.63	5.63 ± 1.14	0
Undeveloped	3.68	4.37	2.60 ± 0.19	5.98 ± 0.45	6.02 ± 1.14	0

the summer dormancy typical of cool-season C3 turf grass lawns (Fry and Huang 2004). Our turf grass FPAR estimates were similar to midsummer values of ~0.7 for a corn and soybean site in Illinois (Turner et al. 2005; Meyers and Hollinger 2004) and a value of ~0.8 for a tallgrass prairie site in eastern Kansas (Turner et al. 2006; Ham and Knapp 1998). Our deciduous broadleaf tree and evergreen needleleaf tree FPAR estimates corresponded well with estimates by Turner et al. (2005) for their respective vegetation types (Wofsy et al. 1993; Anthoni et al. 2002) and with estimates by Turner et al. (2006) for a mixed forest (Davis et al. 2003). Trees did not show as much FPAR variability as did turf grass (Fig. 2), suggesting that trees experienced relatively uniform environmental stress conditions across the metropolitan area but turf grasses had much greater variation in condition, likely due to their more intensive management requirements.

Light use efficiency

We calculated an empirical LUE value for each urban vegetation type using daily GPP and PAR totals from in situ measurements in combination with FPAR values from WV-2 NDVI. The empirical LUE values were applied as constants to produce a single estimate of midsummer GPP. This is in

Table 6 Percent contribution to each land-use type's total GPP (± SD) by vegetation type. The total area (km^2) and the total daily GPP (± area weighted SD; Mg C d^{-1}) of each land-use type are also included

	Contribution (± SD; %) to Land Use GPP					
	Deciduous Broadleaf Tree	Evergreen Needleleaf Tree	Turf Grass	Golf Course Grass	Total Area (km^2)	Total GPP (± SD; Mg C d^{-1})
Total Study Area	27.79 ± 2.75%	6.25 ± 0.56%	59.66 ± 10.52%	6.30 ± 0.64%	894	2071 ± 150
Airport	3.90 ± 0.33%	1.27 ± 0.09%	94.83 ± 20.19%	0%	11	27 ± 5
Golf Course	6.66 ± 0.48%	2.78 ± 0.22%	0%	90.56 ± 9.26%	18	151 ± 11
Industrial	16.52 ± 2.02%	3.61 ± 0.36%	79.87 ± 15.82%	0%	60	72 ± 9
Institutional	16.56 ± 1.83%	3.85 ± 0.40%	79.59 ± 13.15%	0%	54	129 ± 14
Major Highway	8.28 ± 0.97%	1.41 ± 0.16%	90.31 ± 18.18%	0%	37	80 ± 13
Mixed Use	10.33 ± 1.31%	1.93 ± 0.21%	87.74 ± 15.26%	0%	12	19 ± 2
Office	19.16 ± 2.39%	3.56 ± 0.36%	77.28 ± 13.95%	0%	10	13 ± 1
Park, Rec., or Preserve	33.29 ± 2.37%	7.15 ± 0.51%	59.56 ± 9.67%	0%	103	374 ± 19
Residential	33.47 ± 3.47%	7.53 ± 0.69%	59.00 ± 9.57%	0%	424	1106 ± 71
Retail	20.65 ± 2.80%	2.91 ± 0.33%	76.44 ± 15.55%	0%	40	31 ± 4
Undeveloped	28.87 ± 2.10%	6.53 ± 0.49%	64.60 ± 12.25%	0%	57	209 ± 14

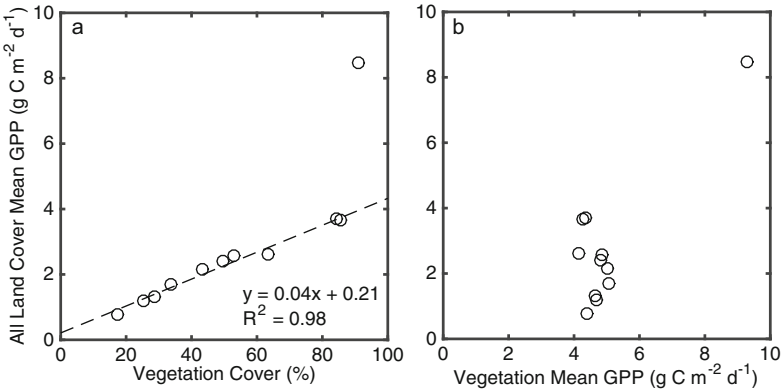

Fig. 7 For each land-use type in this study: (**a**) vegetation cover (%) plotted against mean GPP of all vegetation, impervious and soil (g C m^{-2} d^{-1}), note that golf courses are not included in the linear regression; (**b**) mean GPP of all vegetation types (g C m^{-2} d^{-1}) plotted against mean GPP of all vegetation, impervious and soil (g C m^{-2} d^{-1}). See Tables 4 and 5 for specific land-use values

contrast to global models of GPP, which divide the land surface by biomes or plant functional types, assign a maximum LUE parameter to each class, and then use environmental variables to scale down LUE to account for seasonality and large-scale geographic variability (Song et al. 2013). In this study, in situ GPP measurements for each urban vegetation type allowed us to produce accurate maps of GPP that were representative of clear-sky, midsummer conditions. To extend our map to annual estimates, continuous multi-year flux measurements are available, but a corresponding time series of high spatial resolution imagery is not. However, in future work, data fusion of limited high spatial resolution imagery with daily imagery such as MODIS (e.g., Kim and Hogue 2012) could potentially generate intra- and inter-annual time series of urban FPAR and GPP.

We compared our empirical LUE values to MODIS LUE parameters from the Daily GPP and Annual NPP (MOD17A2/A3) Products User's Guide Version 3.0 (Running and Zhao 2015), which were originally derived in Yang et al. (2007). MOD17 GPP has maximum LUE values for multiple vegetation classes that are reduced by linear ramp functions of minimum daily air temperature and vapor pressure deficit (VPD) based on gridded meteorological data. We used half-hourly air temperature and VPD measurements from our turf site to calculate MOD17 LUE estimates. Using these data, the MOD17 LUE estimates were not affected by minimum air temperature but were affected by VPD. We produced MOD17 LUE estimates using both the mean (2.018 kPa) and the median (1.881 kPa) VPD of our midsummer composite diurnal cycle.

Our empirical LUE values and MOD17 LUE parameters are shown in Table 7. Our deciduous broadleaf tree LUE (0.24 g C MJ^{-1}) was similar to the MOD17 mixed forest LUE (0.23 and 0.31 g C MJ^{-1}). It did not match the MOD17 deciduous broadleaf forest LUE because the latter was scaled to zero due to its VPD threshold. Our evergreen needleleaf tree LUE (0.56 g C MJ^{-1}) was similar to the MOD17 evergreen needleleaf forest LUE (0.63 and 0.66 g C MJ^{-1}). Our turf grass LUE (0.66 g C MJ^{-1}) was in the same range as the MOD17 LUE estimates for the mostly herbaceous vegetation classes of savanna (0.53 and 0.60 g C MJ^{-1}), grassland (0.61 and 0.63 g C MJ^{-1}), and cropland (0.65 and 0.69 g C MJ^{-1}). Our golf course grass LUE (1.14 g C MJ^{-1}) was higher than all MOD17 LUE estimates.

Table 7 Comparison between our empirical LUE estimates and estimates for scaled MODIS GPP (MOD17) LUE by vegetation class. LUE estimates are g C MJ^{-1} PAR

This Study		Estimated MOD17 GPP		
Vegetation Class	LUE	Vegetation Class	LUE (VPD = 2.018 kPa)	LUE (VPD = 1.881 kPa)
Deciduous Broadleaf Tree	0.24	Evergreen Needleleaf Forest	0.63	0.66
		Evergreen Broadleaf Forest	0.60	0.67
Evergreen Needleleaf Tree	0.56	Deciduous Needleleaf Forest	0.19	0.28
		Deciduous Broadleaf Forest	0.00	0.00
		Mixed Forest	0.23	0.31
		Closed Shrubland	0.85	0.89
		Open Shrubland	0.56	0.59
		Woody Savanna	0.57	0.64
Turf Grass	0.66	Savanna	0.53	0.60
Golf Course Grass	1.14	Grassland	0.61	0.63
		Cropland	0.65	0.69

In general, our measured LUE values of urban vegetation were similar to the MOD17 LUE parameters of the corresponding natural vegetation types. However, our results also indicated that caution must be used in applying natural vegetation LUE parameters to estimate urban GPP. For example, we would not have known a priori that our deciduous broadleaf tree LUE would be better represented by the MOD17 mixed forest class rather than the deciduous broadleaf forest class, nor that our measured golf course grass LUE would be underestimated by all the MOD17 vegetation types.

Comparisons between our empirical LUE values and other empirical LUE estimates reported for similar vegetation types are shown in Table 8. The two grass types at our urban study site bracketed the range of published LUE values for natural vegetation, with golf course grass having higher LUE and turf grass having lower LUE compared to natural grasslands. Both of our grass LUE values were lower than the maximum estimates for turf grass LUE at varying levels of nitrogen application (converted using a ratio of NPP/GPP = 0.5; Wu and Bauer 2012). Our evergreen and deciduous tree LUE values were lower than most published values from natural forests. This may be because our LUE estimates were empirically determined for a limited midsummer period, whereas many published values represent maximum LUE for a given vegetation type. Differences apart from maximum LUE most likely reflect the typically lower stem density due to tree spacing in park-like conditions and reduced crown area due to pruning of urban forests compared to natural forest stands (Nowak 1994; Peters and McFadden 2010). Similarly, turf grasses in residential yards are not as uniformly managed as herbaceous crops grown in agricultural settings, and they are less suited to the local climate than prairie tallgrasses. Ruimy et al. (1994) and Ogutu and Dash (2013) provide further LUE comparisons.

Urban GPP compared to natural vegetation

Our mean GPP of 2.64 g C m^{-2} d^{-1} for the total study area (including the large fraction of non-vegetated, impervious surfaces) was lower than GPP estimates for many natural ecosystems (Yuan et al. 2007). Due to similarities in urban land cover composition (McKinney 2006; Groffman et al. 2014), the GPP of the Minneapolis-Saint Paul metropolitan region may have more in common with other midwestern cities than with nearby natural forests and grasslands. The mean GPP of all vegetated areas (*excluding* impervious surfaces) in our total study area was 4.45 g C m^{-2} d^{-1}, which falls at the low end of the range of 5 to 14 g C m^{-2} d^{-1} reported for mixed forests, deciduous broadleaf forests, and grasslands in the same climate zone (Yuan et al. 2007).

Our GPP estimates for deciduous broadleaf trees were lower than many of the values reported in the literature for natural forests (Turner et al. 2005; Yuan et al. 2007; Ogutu and Dash 2013). Reductions in GPP may be because open grown trees, typical of urban areas, tend to have less above ground biomass than trees with similar heights and diameter at breast height measurements in forests (Nowak 1994). Urban trees experience local stresses (Oke 1989) that likely impact evapotranspiration (and thus GPP) per unit area, such as pruning (Hutyra et al. 2011) and upward fluxes of sensible heat and radiation (e.g., from pavement) under street tree canopies (Kjelgren and Montague 1998). Evergreen tree GPP in our study area was similar to estimates from flux measurements at a boreal forest

Table 8 Comparisons of our empirical LUE values to literature values. Literature LUE marked with '*' have been converted to GPP LUE from NPP LUE using a ratio of NPP/GPP = 0.5, and vegetation types denoted with 'max' are maximum LUE parameters that are scaled down by environmental variables to estimate GPP

This Study		Literature		
Vegetation Class	LUE	Vegetation Class	LUE	Reference
Deciduous Broadleaf Tree	0.24	Deciduous Broadleaf Forest	~12	Turner et al. 2005
		Deciduous Broadleaf Forest (max)	1.56	Yang et al. 2007
Evergreen Needleleaf Tree	0.56	Boreal Forest	~1.0	Turner et al. 2005
		Dryland Needleleaf Forest	~0.5	
		Evergreen Needleleaf Forest (max)	1.02	Yang et al. 2007
		Mixed Forest	~1.0	Turner et al. 2006
		Mixed Forest (max)	1.31	Yang et al. 2007
Turf Grass	0.66	Grassland (max)	0.86	Yang et al. 2007
Golf Course Grass	1.14	Cropland (max)	1.47	
		Desert Grassland	~0.5	Turner et al. 2005
		Corn and Soybean (MODIS)	~0.5	
		Corn and Soybean (BigFoot flux model)	~2.0	
		Tallgrass Prairie (MODIS)	~0.5	Turner et al. 2006
		Tallgrass Prairie (BigFoot flux model)	~1.5	
		Turf Grass (high N; max)	2.16*	Wu and Bauer 2012
		Turf Grass (med. N; max)	1.68*	
		Turf Grass (low N; max)	1.3*	

site in northern Manitoba at the peak daily rate (Goulden et al. 1997; Turner et al. 2005; Heinsch et al. 2006). While there is no direct analogue for turf grass in natural ecosystems, turf grass GPP can be compared to estimates for grasslands and herbaceous crops. Turf grass GPP estimates were similar to GPP estimates at an abandoned agricultural field near Duke Forest in North Carolina (Novick et al. 2004; Yuan et al. 2007), but were lower than GPP estimated at a tallgrass prairie site in Kansas (Song et al. 2005; Yuan et al. 2007) and a corn and soybean site in Illinois (Meyers and Hollinger 2004; Turner et al. 2005). By contrast, our golf course grass GPP was similar to the latter two sites.

Spatial variability of GPP

Variability within vegetation types

Our GPP variability within the vegetation type classes was driven by spatial variations in FPAR because our empirical LUE parameters were constant within a given vegetation type and we assumed a uniform incident PAR for clear-sky conditions across our study area. The spatial variations in FPAR were determined by the amount of leaf area and canopy condition, which modulate the absorption of PAR. This is one of the first studies of urban GPP to examine its variability within different vegetation types, including turf grass lawns, golf course grass, deciduous broadleaf trees, and evergreen needleleaf trees. This was possible because the 2 m resolution imagery from WV-2 and the 1 m gridded LiDAR canopy height data allowed us to resolve individual tree crowns and small lawn patches across the entire metropolitan area.

We found that the spatial variability of GPP within the turf grass class was larger than all the other vegetation types, and this was likely partially attributable to differences in lawn management, such as fertilization, aeration, and irrigation, that can increase GPP in turf grass (Milesi et al. 2005; Polsky et al. 2014). On the other hand, even at the 2 m resolution of our imagery, low maintenance lawns form a matrix with small patches of bare soil included within pixels that are classified as "pure" turf grass vegetation, reducing GPP estimates. This effect must have been expressed in our results because our GPP estimates were produced for midsummer, when cool-season C3 turf grasses normally have a period of dormancy due to high temperatures (Peters et al. 2011). Taken together, these factors alternatively favored the high or the low ends of the GPP range, which is consistent with the overall higher spatial variability within turf grass compared to the other vegetation types.

The golf course grass, deciduous broadleaf tree, and evergreen needleleaf tree classes all had similar spatial variability in GPP, as measured by CV. Golf course grasses can be expected to have more uniformly high maintenance, with significant nutrient inputs through fertilizers and intensive irrigation to reduce the stress of midsummer high temperatures on the grass (Qian and Follett 2002; Peters et al. 2011). Trees do not experience the heat-induced dormancy of the C3 turf grasses, and tree LAI changed little in the midsummer period we studied (Peters and McFadden 2010). Additionally, the lower spatial variability in tree-covered areas, as evidenced by FPAR, may have been due to NDVI saturation in dense canopies (Huete 1988). The spatial variability of GPP would likely be more pronounced if trees were distinguished by species rather than plant functional type (Ahl et al. 2004; Peters and McFadden 2012).

Variability among land-use types

Our study allowed us to separate the effects of vegetation percent cover and vegetation condition because we were able to map individual tree and turf grass patches using high spatial resolution imagery. This minimizes the number of mixed vegetation pixels, and the FPAR can more accurately represent spatial variations in the condition of "pure" pixels of each vegetation type. This adds new information to previous reports on urban GPP using coarser resolution imagery such as Landsat, in which GPP could be estimated only at the level of broad urban density classes or land-use types (e.g., Zhao et al. 2007). Here, we could examine why GPP differs among urban land-use types due to percent vegetation cover and differences in the GPP rates. The mean GPP of the major urban land-use types had a strong linear relationship with percent vegetation cover, with the exception of the golf course class (Fig. 7a). In contrast, the mean rate of GPP of only the vegetated pixels did not explain the variations of GPP among land-use types (Fig. 7b).

While percent vegetation cover was most important in explaining differences among land-use types at the scale of the metropolitan region, both percent cover and the mean rate of GPP were important for understanding patterns within specific land-use types. For example, residential land use covered nearly 50% of the total area of our study region and accounted for the largest share of the region's total GPP (Table 6). The rate of turf grass GPP was higher in residential areas compared to all land-use types other than parks, recreational areas, or preserves. The high rate of GPP in residential areas may have been due to more intensive management including fertilizer application and irrigation (Milesi et al. 2005).

Highly vegetated land-use classes, including parks, recreational areas, or preserves; undeveloped lands; and golf courses had higher mean GPP than did residential land, but they covered a smaller area. Parks, recreational areas, or preserves and undeveloped areas had the highest estimates of mean GPP for deciduous broadleaf trees. The higher rates of GPP in these highly vegetated land-use types could be because of reduced plant water stress due to lower temperatures and lower vapor

pressure deficit (Kjelgren and Montague 1998; Spronken-Smith et al. 2000).

The land-use classes with high impervious surface cover had low total GPP mainly due to their relative lack of vegetation, but the mean rate of GPP per unit area of vegetation was also slightly lower compared to the more highly vegetated land-use types. The lower rate of GPP was consistent with plant water stress in more open, warm sites. Field experiments with well-watered plants have shown that isolated plants surrounded by impervious surfaces tend to have much higher transpiration rates than do less isolated plants (Hagishima et al. 2007). Without sufficient irrigation, C3 turf grasses are GPP-limited at high levels of potential evapotranspiration and temperature (Peters and McFadden 2012). Another possibility is that the less vegetated areas had more pixels mixed with impervious surfaces, which would reduce the apparent GPP due to the effect on NDVI (Wetherley et al. 2017). This effect should have been limited at the high spatial resolution used in our study, but even with the 2 m resolution of the WV-2 imagery there undoubtedly were some effects due to mixtures of bare soil within turf grass lawns or tree canopies above pavement, for example.

Finally, along a gradient of land-use types from low to high percent total vegetation cover, we observed that the main urban vegetation types followed two different patterns (Fig. 6). Turf grass cover increased with total vegetation percent cover, except in the three land-use types where trees were most important—parks, undeveloped, and residential—in which turf grass cover was reduced as tree cover increased. By contrast, deciduous broadleaf tree cover remained at a nearly constant level of 6–8% in nearly all land-use types having <50% total vegetation cover, then increased in a step-like manner to levels of 35–47% in the land-use types in which trees were most important.

This suggests two generalizations about the contributions to regional GPP. First, there was a relatively constant minimum of tree canopy cover across land-use types, perhaps occurring as street trees. Second, much of the linear increase of GPP in relation to increasing total vegetation cover was due to a steadily increasing amount of turf grass cover. This suggests that, due to the high GPP of turf grass compared to deciduous broadleaf trees, GPP of most land-use types in the metropolitan area would be highly sensitive to changes in turf grass percent cover or maintenance, for example through changes in planting preferences or regulations on landscape irrigation. The effects of trees would be most important in: park, recreational, or preserve; undeveloped; and residential.

Implications for net carbon budget of urban vegetation and soils

This study quantified GPP, the initial input of atmospheric carbon to ecosystems, because it is an important metric of ecosystem function and is amenable to estimation from satellite imagery to improve our understanding of how vegetation carbon uptake varies spatially across a large metropolitan region. In residential land use, covering 47.4% of the region, flux partitioning analyses of our flux tower data have shown that during the growing season GPP can have a larger magnitude than any other component of the urban carbon budget, including anthropogenic emissions (Menzer and McFadden 2017). On the other hand, GPP is small in urban land-use types with little vegetation and, in our cold continental study area, it reduces to zero everywhere during the winter. Importantly, GPP always is balanced by a flux of similar magnitude, but of the opposite sign, in the form of ecosystem respiration (the combined respiration of plants and soil microorganisms). This can result in a *net* carbon flux from urban vegetation and soils that is a small fraction (<10%) of GPP (Menzer and McFadden 2017). This means that while quantifying GPP is necessary to understand patterns of carbon uptake by vegetation in urban ecosystems, high rates of GPP do not necessarily imply high rates of net carbon storage.

We found turf grasses had higher midsummer LUE than trees and that differences in turf grass cover were responsible for much of the variation in total vegetation cover among land-use types. However, in our flux studies, turf grass ecosystems were often net sources of atmospheric CO_2 during midsummer due to temperature-induced dormancy, resulting in high rates of ecosystem respiration that exceeded GPP (Peters and McFadden 2012). On an annual basis, our turf grass flux study site was a small net sink of −71 g C m^{-2} y^{-1} in 2008 with typical temperature and moisture conditions, but it was a net source of 92 g C m^{-2} y^{-1} in 2007 with relatively hot, dry summertime conditions (Hiller et al. 2011; Peters and McFadden 2012). This is perhaps unsurprising given that these turf grass fields, similar to residential lawns in the area, were mowed weekly with the clippings left to decompose on the surface. While a significant amount of GPP is represented in the growing turf grass leaves, most of the carbon is returned to the atmosphere by the decomposition of the clippings and root respiration. At the same time, while natural ecosystems such as tallgrass prairie can take up large amounts of carbon in soil organic matter over time (Suyker and Verma 2001), in urban turf grass shallow rooting depths and maintenance practices such as aeration limit the amount of soil organic matter that can be stored (Fry and Huang 2004). Although well-irrigated areas tend to produce greater initial sinks through greater biomass production (Milesi et al. 2005), areas of lower maintenance (e.g., certain residential areas) may produce greater sinks in soil over time than highly managed recreational areas (Pouyat et al. 2006).

Deciduous and evergreen tree species at our sites were consistent net annual carbon sinks (Peters and McFadden 2012). Trees store carbon as wood (Nowak 1994) in addition to producing soil organic matter, and have greater long term

carbon storage with about half of forest GPP going into net primary production (NPP) (DeLucia et al. 2007). However, there is high variability in this conversion efficiency due to many factors including stand age (Noormets et al. 2007) and local temperature reduction (Peters and McFadden 2010). Although spatial modeling of plant respiration and NPP was beyond the scope of this study, we note that in our study area net carbon uptake over time was likely to be mainly driven by trees rather than turf grasses. Thus we expect that the land-use types with high tree cover will have a larger effect on the net carbon exchange of urban vegetation as compared to turf grass-dominated land-use types, despite the latter's larger GPP.

Broader implications of high spatial resolution urban carbon flux measurements

The continued development of satellites that can provide high spatial resolution imagery at sufficient spectral resolutions (e.g., WorldView-4), and the increased availability of LiDAR data over cities, have several implications for carbon flux studies in urban areas. First, high spatial resolution imagery allows for fine-scale image objects, such as lawns and tree canopies, to be uniquely identified, which provides increased accuracy in carbon flux attribution. Second, it creates opportunities for comparisons not only among but also *within* urban spatial units such as land-use types (as in this study), neighborhoods, census tracts, parks, households, and individual trees. Third, it allows for improved spatial estimation of key variables used in quantifying ecosystem services and carbon accounting, especially when fused with LiDAR data (e.g., Alonzo et al. 2016). Lastly, with repeated observations, it could provide opportunities for tracking fine-scale urban development and vegetation functioning through time. There are limits to the utility of improved spatial resolution at extremely fine scales, but in general, these data allow for more accurate and spatially robust measurements of carbon fluxes both across and within urban areas as compared with coarser resolution remote sensing measurements.

Conclusions

We analyzed variations in GPP across the 894 km^2 Minneapolis-Saint Paul metropolitan region. The vegetation cover of the total study area was 52.1% including all land cover classes, while the tree canopy cover was 28.0%. Our results demonstrated that high spatial resolution imagery can reveal important patterns of spatial variability in urban GPP compared to lower resolution data. However, the total percent vegetation cover provided reasonable estimates of GPP at large scales because vegetation composition was quite consistent across the study area. This suggests that urban GPP can be adequately quantified at the metropolitan scale using coarser resolution sensors and fractional vegetation cover estimates given that vegetation LUE is appropriately parameterized, but higher resolution imagery is necessary to compare within and among neighborhoods, land-use types, and vegetation cover classes.

For the total study area, the mean GPP per unit land area (including vegetation, impervious surfaces, and soil) was 2.64 g C m^{-2} d^{-1}. Our mapped estimate of vegetation GPP was 11.4% less than the GPP determined from CO_2 flux measurements when both were compared over the footprint area of a tall eddy covariance tower. The mean estimates of GPP were largely constant within the vegetation classes across the selected regions. For the total study area, deciduous broadleaf trees had the lowest mean GPP (2.52 g C m^{-2} d^{-1}), evergreen needleleaf trees (5.81 g C m^{-2} d^{-1}) and turf grass (6.05 g C m^{-2} d^{-1}) had similar means, and golf course grass (11.77 g C m^{-2} d^{-1}) had the highest mean GPP. The contributions to total GPP by vegetation class were consistent across the study region, with turf grass contributing 55–62% and deciduous broadleaf trees contributing 27–32% of the total GPP. Both classes had similar percent cover in the study region, but the lower LUE of the deciduous broadleaf trees resulted in a lower contribution to the total GPP.

This is one of the first studies of urban GPP to examine its spatial variability within different vegetation types. This was possible because the 2 m imagery from WV-2 and the 1 m gridded LiDAR canopy height data set allowed us to resolve individual tree crowns and small lawn patches across an entire metropolitan area. We found that the variability of GPP within the turf grass class was larger, with a CV that was nearly twice as large, compared to all of the other vegetation types. The larger spatial variability was likely attributable to differences in lawn management, such as fertilization, aeration, and irrigation, that can significantly increase GPP in turf grass. We also examined why GPP differs among urban land-use types due to their percent vegetation cover versus differences in the rate of GPP from place to place. The GPP of the major urban land-use types had a strong linear relationship with percent vegetation cover, with the exception of the golf courses. In contrast, the mean rate of GPP of only the vegetated pixels did not explain the variations of GPP among land-use types because it varied within a narrow range from 4.12 to 5.04 g C m^{-2} d^{-1}.

Over the total area, urban GPP tended to be low relative to natural forests and grasslands due to reduced total vegetation cover. The mean GPP of all vegetated areas (*excluding* impervious surfaces) in our total study area was 4.45 g C m^{-2} d^{-1}, which falls at the low end of the range of 5 to 14 g C m^{-2} d^{-1} reported for mixed forests, deciduous broadleaf forests, and grasslands in the same climate zone. It is important to note that these comparisons refer strictly to GPP, which was the focus of our study. When taking plant and soil respiration into

account (i.e., NPP or net ecosystem exchange of CO_2), our in situ flux data showed that, on an annual basis, turf grass (which had higher GPP than trees) could be a net source or a sink of carbon, while trees were consistently net carbon sinks. Further work would use remote sensing data fusion techniques to evaluate seasonal changes in the spatial variability of GPP by vegetation and land-use type, and would help to extrapolate our current results to an annual cycle.

Acknowledgements The field measurements at KUOM were funded by a grant from the NASA Earth Science Division (NNG04GN80G) as a component of the North American Carbon Program (NACP), and the acquisition of the WorldView-2 imagery was funded by a grant from the NSF Dynamics of Coupled Natural and Human Systems Program (BCS-0908549).

Compliance with ethical standards

Competing interests None declared.

References

Adler-Golden S, Berk A, Bernstein LS et al (1998) FLAASH, a MODTRAN4 atmospheric correction package for hyperspectral data retrievals and simulations. In: Green RO (ed) Summaries of the seventh JPL airborne earth science workshop January 12–16, 1998. Jet Propulsion Laboratory, California Institute of Technology, Pasadena, California, pp 9–14

Ahl DE, Gower ST, Mackay DS, Burrows SN, Norman JM, Diak GR (2004) Heterogeneity of light use efficiency in a northern Wisconsin forest: implications for modeling net primary production with remote sensing. Remote Sens Environ 93:168–178. https://doi.org/10.1016/j.rse.2004.07.003

Akbari H, Rose LS, Taha H (2003) Analyzing the land cover of an urban environment using high-resolution orthophotos. Landsc Urban Plan 63:1–14. https://doi.org/10.1016/S0169-2046(02)00165-2

Alonzo M, McFadden JP, Nowak DJ, Roberts DA (2016) Mapping urban forest structure and function using hyperspectral imagery and lidar data. Urban For Urban Green 17:135–147. https://doi.org/10.1016/j.ufug.2016.04.003

Anthoni PM, Unsworth MH, Law BE, Irvine J, Baldocchi DD, Tuyl SV, Moore D (2002) Seasonal differences in carbon and water vapor exchange in young and old-growth ponderosa pine ecosystems. Agric For Meteorol 111:203–222. https://doi.org/10.1016/S0168-1923(02)00021-7

As-syakur AR, Osawa T, Adnyana IWS (2010) Medium spatial resolution satellite imagery to estimate gross primary production in an urban area. Remote Sens 2:1496–1507. https://doi.org/10.3390/rs2061496

Baldocchi DD (2008) "Breathing" of the terrestrial biosphere: lessons learned from a global network of carbon dioxide flux measurement systems. Aust J Bot 56:1–26. https://doi.org/10.1071/BT07151

Bergeron O, Strachan IB (2011) CO2 sources and sinks in urban and suburban areas of a northern mid-latitude city. Atmos Environ 45:1564–1573. https://doi.org/10.1016/j.atmosenv.2010.12.043

Buyantuyev A, Wu J (2009) Urbanization alters spatiotemporal patterns of ecosystem primary production: a case study of the Phoenix metropolitan region, USA. J Arid Environ 73:512–520. https://doi.org/10.1016/j.jaridenv.2008.12.015

Cadenasso ML, Pickett STA, Schwarz K (2007) Spatial heterogeneity in urban ecosystems: reconceptualizing land cover and a framework for classification. Front Ecol Environ 5:80–88. https://doi.org/10.1890/1540-9295(2007)5[80:SHIUER]2.0.CO;2

Chapin FS, Matson PA, Mooney HA (2002) Principles of terrestrial ecosystem ecology. Springer-Verlag, New York

Davis KJ, Bakwin PS, Yi C et al (2003) The annual cycles of CO2 and H2O exchange over a northern mixed forest as observed from a very tall tower. Glob Chang Biol 9:1278–1293. https://doi.org/10.1029/2009JD012832

DeLucia EH, Drake JE, Thomas RB, Gonzalez-Meler M (2007) Forest carbon use efficiency: is respiration a constant fraction of gross primary production? Glob Chang Biol 13:1157–1167. https://doi.org/10.1111/j.1365-2486.2007.01365.x

Fry J, Huang B (2004) Applied turfgrass science and physiology. John Wiley and Sons, Hoboken

Fugro Horizons, Inc. and the Minnesota Department of Natural Resources (2012) LiDAR elevation, twin cities metro region, Minnesota, 2011. Minnesota Department of Natural Resources, St. Paul, Minnesota

Goulden ML, Daube BC, Fan S-M, Sutton DJ, Bazzaz A, Munger JW, Wofsy SC (1997) Physiological responses of a black spruce forest to weather. J Geophys Res 102:28987–28996. https://doi.org/10.1029/97JD01111

Green RO, Eastwood ML, Sarture CM, Chrien TG, Aronsson M, Chippendale BJ, Faust JA, Pavri BE, Chovit CJ, Solis M, Olah MR, Williams O (1998) Imaging spectroscopy and the airborne visible/infrared imaging spectrometer (AVIRIS). Remote Sens Environ 65:227–248. https://doi.org/10.1016/S0034-4257(98)00064-9

Grimm NB, Faeth SH, Golubiewski NE, Redman CL, Wu J, Bai X, Briggs JM (2008) Global change and the ecology of cities. Science 319:756–760. https://doi.org/10.1126/science.1150195

Groffman PM, Cavender-Bares J, Bettez ND, Grove JM, Hall SJ, Heffernan JB, Hobbie SE, Larson KL, Morse JL, Neill C, Nelson K, O'Neil-Dunne J, Ogden L, Pataki DE, Polsky C, Chowdhury RR, Steele MK (2014) Ecological homogenization of urban USA. Front Ecol Environ 12:74–81. https://doi.org/10.1890/120374

Hagishima A, Narita KI, Tanimoto J (2007) Field experiment on transpiration from isolated urban plants. Hydrol Process 21:1217–1222. https://doi.org/10.1002/hyp.6681

Ham JM, Knapp AK (1998) Fluxes of CO2 water vapor, and energy from a prairie ecosystem during the seasonal transition from carbon sink to carbon source. Agric For Meteorol 89:1–14. https://doi.org/10.1016/S0168-1923(97)00062-2

Hardiman BS, Wang JA, Hutyra LR, Gately CK, Getson JM, Friedl MA (2017) Accounting for urban biogenic fluxes in regional carbon budgets. Sci Total Environ 592:366–372. https://doi.org/10.1016/j.scitotenv.2017.03.028

Hedblom M, Lindberg F, Vogel E, Wissman J, Ahrné K (2017) Estimating urban lawn cover in space and time: case studies in three Swedish cities. Urban Ecosyst 20:1109–1119. https://doi.org/10.1007/s11252-017-0658-1

Heinsch FA, Running SW, Kimball JS et al (2006) Evaluation of remote sensing based terrestrial productivity from MODIS using regional tower eddy flux network observations. IEEE Trans Geosci Remote Sens 44:1908–1925. https://doi.org/10.1109/TGRS.2005.853936

Herold M, Roberts DA, Gardner ME, Dennison PE (2004) Spectrometry for urban area remote sensing - development and analysis of a spectral library from 350 to 2400 nm. Remote Sens Environ 91:304–319. https://doi.org/10.1016/j.rse.2004.02.013

Hilker T, Coops NC, Wulder MA, Black TA, Guy RD (2008) The use of remote sensing in light use efficiency based models of gross primary production: a review of current status and future requirements. Sci Total Environ 404:411–423. https://doi.org/10.1016/j.scitotenv.2007.11.007

Hiller RV, McFadden JP, Kljun N (2011) Interpreting CO2 fluxes over a suburban Lawn: the influence of traffic emissions. Boundary-Layer Meteorol 138:215–230. https://doi.org/10.1007/s10546-010-9558-0

Huete AR (1988) A soil-adjusted vegetation index (SAVI). Remote Sens Environ 25:295–309. https://doi.org/10.1016/0034-4257(88)90106-X

Hutyra LR, Yoon B, Alberti M (2011) Terrestrial carbon stocks across a gradient of urbanization: a study of the Seattle, WA region. Glob Chang Biol 17:783–797. https://doi.org/10.1111/j.1365-2486.2010.02238.x

Imhoff ML, Bounoua L, DeFries R, Lawrence WT, Stutzer D, Tucker CJ, Ricketts T (2004) The consequences of urban land transformation on net primary productivity in the United States. Remote Sens Environ 89:434–443. https://doi.org/10.1016/j.rse.2003.10.015

Järvi L, Nordbo A, Junninen H, Riikonen A, Moilanen J, Nikinmaa E, Vesala T (2012) Seasonal and annual variation of carbon dioxide surface fluxes in Helsinki, Finland, in 2006-2010. Atmos Chem Phys 12:8475–8489. https://doi.org/10.5194/acp-12-8475-2012

Jia X, Richards JA (1994) Efficient maximum likelihood classification for imaging spectrometer data sets. IEEE Trans Geosci Remote Sens 32:274–281. https://doi.org/10.1109/36.295042

Kim J, Hogue TS (2012) Evaluation and sensitivity testing of a coupled Landsat-MODIS downscaling method for land surface temperature and vegetation indices in semi-arid regions. J Appl Remote Sens 6:63569. https://doi.org/10.1117/1.JRS.6.063569

Kjelgren R, Montague T (1998) Urban tree transpiration over turf and asphalt surfaces. Atmos Environ 32:35–41. https://doi.org/10.1016/S1352-2310(97)00177-5

Kljun N, Calanca P, Rotachhi MW, Schmid HP (2004) A simple parameterisation for flux footprint predictions. Boundary-Layer Meteorol 112:503–523. https://doi.org/10.1023/B:BOUN.0000030653.71031.96

Kordowski K, Kuttler W (2010) Carbon dioxide fluxes over an urban park area. Atmos Environ 44:2722–2730. https://doi.org/10.1016/j.atmosenv.2010.04.039

McKinney ML (2006) Urbanization as a major cause of biotic homogenization. Biol Conserv 127:247–260. https://doi.org/10.1016/j.biocon.2005.09.005

Menzer O, McFadden JP (2017) Statistical partitioning of a three-year time series of direct urban net CO 2 flux measurements into biogenic and anthropogenic components. Atmos Environ 170:319–333. https://doi.org/10.1016/j.atmosenv.2017.09.049

Menzer O, Meiring W, Kyriakidis PC, McFadden JP (2015) Annual sums of carbon dioxide exchange over a heterogeneous urban landscape through machine learning based gap-filling. Atmos Environ 101:312–327. https://doi.org/10.1016/j.atmosenv.2014.11.006

Metropolitan Council (2011) Generalized land use 2010 for the twin cities metropolitan area. Metropolitan Council, St. Paul, Minnesota

Metropolitan Council (2013) Lakes and rivers – open water features. Metropolitan Council, St. Paul, Minnesota

Metropolitan Council (2015) MetroStats report. The twin cities region's local forecasts. Metropolitan Council. https://metrocouncil.org/Data-and-Maps/Publications-And-Resources/MetroStats/Land-Use-and-Development/The-Twin-Cities-Region-s-Local-Forecasts.aspx. Accessed 31 May 2018

Metropolitan Mosquito Control District (2012) Metro Wetlands and Wet Areas (MMCD). Metropolitan Mosquito Control District, St. Paul, Minnesota

Meyers TP, Hollinger SE (2004) An assessment of storage terms in the surface energy balance of maize and soybean. Agric For Meteorol 125:105–115. https://doi.org/10.1016/j.agrformet.2004.03.001

Milesi C, Elvidge CD, Nemani RR, Running SW (2003) Assessing the impact of urban land development on net primary productivity in the southeastern United States. Remote Sens Environ 86:401–410. https://doi.org/10.1016/S0034-4257(03)00081-6

Milesi C, Running SW, Elvidge CD, Dietz JB, Tuttle BT, Nemani RR (2005) Mapping and modeling the biogeochemical cycling of turf grasses in the United States. Environ Manag 36:426–438. https://doi.org/10.1007/s00267-004-0316-2

Minnesota Department of Natural Resources and Surdex Corporation (2010) Digital orthoimagery, twin cities, spring 2010, 1-ft resolution. Minnesota Department of Natural Resources, St. Paul

Monteith JL (1972) Solar radiation and productivity in tropical ecosystems. J Appl Ecol 9:747–766. https://doi.org/10.2307/2401901

Myeong S, Nowak DJ, Hopkins PF, Brock RH (2001) Urban cover mapping using digital, high-spatial resolution aerial imagery. Urban Ecosyst 5:243–256. https://doi.org/10.1023/A:1025687711588

Myint SW, Gober P, Brazel A, Grossman-Clarke S, Weng Q (2011) Per-pixel vs. object-based classification of urban land cover extraction using high spatial resolution imagery. Remote Sens Environ 115:1145–1161. https://doi.org/10.1016/j.rse.2010.12.017

Noormets A, Chen J, Crow TR (2007) Age-dependent changes in ecosystem fluxes in managed forests in northern Wisconsin, USA. Ecosystems 10:187–203. https://doi.org/10.1007/s10021-007-9018-y

Novick KA, Stoy PC, Katul GG, Ellsworth DS, Siqueira MBS, Juang J, Oren R (2004) Carbon dioxide and water vapor exchange in a warm temperate grassland. Oecologia 138:259–274. https://doi.org/10.1007/s00442-003-1388-z

Nowak DJ (1994) Atmospheric carbon dioxide reduction by Chicago's urban forest. In: EG MP, Nowak DJ, Rowntree RA (eds) Chicago's urban Forest ecosystem: results of the Chicago urban Forest ecosystem. USDA Forest Service general technical report NE-186, Radnor, pp 83–94

Nowak DJ, Crane DE, Stevens JC (2006) Air pollution removal by urban trees and shrubs in the United States. Urban For Urban Green 4:115–123. https://doi.org/10.1016/j.ufug.2006.01.007

Ogutu BO, Dash J (2013) Assessing the capacity of three production efficiency models in simulating gross carbon uptake across multiple biomes in conterminous USA. Agric For Meteorol 174–175:158–169. https://doi.org/10.1016/j.agrformet.2013.02.016

Oke TR (1989) The micrometeorology of the urban forest. Philos Trans R Soc B Biol Sci 324:335–349. https://doi.org/10.1098/rstb.1989.0051

Pataki DE, Alig RJ, Fung AS et al (2006) Urban ecosystems and the north American carbon cycle. Glob Chang Biol 12:2092–2102. https://doi.org/10.1111/j.1365-2486.2006.01242.x

Peters EB, McFadden JP (2010) Influence of seasonality and vegetation type on suburban microclimates. Urban Ecosyst 13:443–460. https://doi.org/10.1007/s11252-010-0128-5

Peters EB, McFadden JP (2012) Continuous measurements of net CO2 exchange by vegetation and soils in a suburban landscape. J Geophys Res Biogeosci 117:G03005. https://doi.org/10.1029/2011JG001933

Peters EB, Hiller RV, McFadden JP (2011) Seasonal contributions of vegetation types to suburban evapotranspiration. J Geophys Res Biogeosci 116:1–16. https://doi.org/10.1029/2010JG001463

Polsky C, Grove JM, Knudson C, Groffman PM, Bettez N, Cavender-Bares J, Hall SJ, Heffernan JB, Hobbie SE, Larson KL, Morse JL, Neill C, Nelson KC, Ogden LA, O'Neil-Dunne J, Pataki DE, Roy Chowdhury R, Steele MK (2014) Assessing the homogenization of urban land management with an application to US residential lawn care. Proc Natl Acad Sci 111:4432–4437. https://doi.org/10.1073/pnas.1323995111

Potapenko J (2014) High-resolution LiDAR Pointcloud data processing, computation, and visualization with application to the Erosion analysis of the California Channel islands. Thesis, University of California Santa Barbara

Pouyat RV, Yesilonis ID, Nowak DJ (2006) Carbon storage by urban soils in the United States. J Environ Qual 35:1566–1575. https://doi.org/10.2134/jeq2005.0215

Qian YL, Follett RF (2002) Assessing soil carbon sequestration in turfgrass systems using long-term soil testing data. Agron J 94:930–935. https://doi.org/10.2134/agronj2002.9300

Raciti SM, Hutyra LR, Newell JD (2014) Mapping carbon storage in urban trees with multi-source remote sensing data: relationships between biomass, land use, and demographics in Boston neighborhoods. Sci Total Environ 500–501:72–83. https://doi.org/10.1016/j.scitotenv.2014.08.070

Reichstein M, Falge E, Baldocchi D, Papale D, Aubinet M, Berbigier P, Bernhofer C, Buchmann N, Gilmanov T, Granier A, Grunwald T, Havrankova K, Ilvesniemi H, Janous D, Knohl A, Laurila T, Lohila A, Loustau D, Matteucci G, Meyers T, Miglietta F, Ourcival J-M, Pumpanen J, Rambal S, Rotenberg E, Sanz M, Tenhunen J, Seufert G, Vaccari F, Vesala T, Yakir D, Valentini R (2005) On the separation of net ecosystem exchange into assimilation and ecosystem respiration: review and improved algorithm. Glob Chang Biol 11(9):1424–1439

Ruimy A, Saugier B, Dedieu G (1994) Methodology for the estimation of terrestrial net primary production from remotely sensed data. J Geophys Res Atmos 99:5263–5283. https://doi.org/10.1029/93JD03221

Running SW, Zhao M (2015) User's guide daily GPP and annual NPP (MOD17A2/A3) products NASA earth observing system MODIS land algorithm version 3.0 for collection 6. 1–28

Sen Roy S, Yuan F (2009) Trends in extreme temperatures in relation to urbanization in the Twin Cities metropolitan area , Minnesota. J Appl Meteorol Climatol 43:669–679. https://doi.org/10.1175/2008JAMC1983.1

Seto KC, Güneralp B, Hutyra LR (2012) Global forecasts of urban expansion to 2030 and direct impacts on biodiversity and carbon pools. Proc Natl Acad Sci U S A 109:16083–16088. https://doi.org/10.1073/pnas.1211658109

Sims DA, Luo HY, Hastings S et al (2006) Parallel adjustments in vegetation greenness and ecosystem CO2 exchange in response to drought in a Southern California chaparral ecosystem. Remote Sens Environ 103:289–303. https://doi.org/10.1016/j.rse.2005.01.020

Soegaard H, Møller-Jensen L (2003) Towards a spatial CO2 budget of a metropolitan region based on textural image classification and flux measurements. Remote Sens Environ 87:283–294. https://doi.org/10.1016/S0034-4257(03)00185-8

Song J, Liao K, Coulter RL, Lesht BM (2005) Climatology of the low-level jet at the southern Great Plains atmospheric boundary layer experiments site. J Appl Meteorol 44:1593–1606. https://doi.org/10.1175/JAM2294.1

Song C, Dannenberg MP, Hwang T (2013) Optical remote sensing of terrestrial ecosystem primary productivity. Prog Phys Geogr 37:834–854. https://doi.org/10.1177/0309133313507944

Spronken-Smith RA, Oke TR, Lowry WP (2000) Advection and the surface energy balance across an irrigated urban park. Int J Climatol 20:1033–1047. https://doi.org/10.1002/1097-0088(200007)20:9<1033::AID-JOC508>3.3.CO;2-L

Strohbach MW, Haase D (2012) Above-ground carbon storage by urban trees in Leipzig, Germany: analysis of patterns in a European city. Landsc Urban Plan 104:95–104. https://doi.org/10.1016/j.landurbplan.2011.10.001

Suyker AE, Verma SB (2001) Year-round observations of the net ecosystem exchange of carbon dioxide in a native tallgrass prairie. Glob Chang Biol 7:279–289. https://doi.org/10.1046/j.1365-2486.2001.00407.x

Tigges J, Churkina G, Lakes T (2017) Modeling above-ground carbon storage: a remote sensing approach to derive individual tree species information in urban settings. Urban Ecosyst 20:97–111. https://doi.org/10.1007/s11252-016-0585-6

Todhunter PE (1996) Environmental indices for the twin cities metropolitan area (Minnesota, USA) urban heat island - 1989. Clim Res 6:59–69

Tucker CJ (1979) Red and photographic infrared linear combinations for monitoring vegetation. Remote Sens Environ 8:127–150. https://doi.org/10.1016/0034-4257(79)90013-0

Turner DP, Ritts WD, Cohen WB, Maeirsperger TK, Gower ST, Kirschbaum AA, Running SW, Zhao M, Wofsy SC, Dunn AL, Law BE, Campbell JL, Oechel WC, Kwon HJ, Meyers TP, Small EE, Kurc SA, Gamon JA (2005) Site-level evaluation of satellite-based global terrestrial gross primary production and net primary production monitoring. Glob Chang Biol 11:666–684. https://doi.org/10.1111/j.1365-2486.2005.00936.x

Turner DP, Ritts WD, Cohen WB, Gower ST, Running SW, Zhao M, Costa MH, Kirschbaum AA, Ham JM, Saleska SR, Ahl DE (2006) Evaluation of MODIS NPP and GPP products across multiple biomes. Remote Sens Environ 102:282–292. https://doi.org/10.1016/j.rse.2006.02.017

Wetherley EB, Roberts DA, McFadden JP (2017) Mapping spectrally similar urban materials at sub-pixel scales. Remote Sens Environ 195:170–183. https://doi.org/10.1016/j.rse.2017.04.013

Winkler JA, Skaggs RH, Baker DG (1981) Effect of temperature adjustments on the Minneapolis-St. Paul urban heat island J Appl Meteorol 20:1295–1300. https://doi.org/10.1175/1520-0450(1981)020<1295:EOTAOT>2.0.CO;2

Wofsy SC, Goulden ML, Munger JW et al (1993) Net exchange of CO_2 in a mid-latitude forest. Science 260(5112):1314–1317. https://doi.org/10.1126/science.260.5112.1314

Wu J, Bauer ME (2012) Estimating net primary production of turfgrass in an urban-suburban landscape with QuickBird imagery. Remote Sens 4:849–866. https://doi.org/10.3390/rs4040849

Wu C, Chen JM, Desai AR, Hollinger DY, Arain MA, Margolis HA, Gough CM, Staebler RM (2012) Remote sensing of canopy light use efficiency in temperate and boreal forests of North America using MODIS imagery. Remote Sens Environ 118:60–72. https://doi.org/10.1016/j.rse.2011.11.012

Yang F, Ichii K, White MA, Hashimoto H, Michaelis AR, Votava P, Zhu AX, Huete A, Running SW, Nemani RR (2007) Developing a continental-scale measure of gross primary production by combining MODIS and AmeriFlux data through support vector machine approach. Remote Sens Environ 110:109–122. https://doi.org/10.1016/j.rse.2007.02.016

Yuan F, Sawaya KE, Loeffelholz BC, Bauer ME (2005) Land cover classification and change analysis of the twin cities (Minnesota) metropolitan area by multitemporal Landsat remote sensing. Remote Sens Environ 98:317–328. https://doi.org/10.1016/j.rse.2005.08.006

Yuan W, Liu S, Zhou G, Zhou G, Tieszen LL, Baldocchi D, Bernhofer C, Gholz H, Goldstein AH, Goulden ML, Hollinger DY, Hu Y, Law BE, Stoy PC, Vesala T, Wofsy SC (2007) Deriving a light use efficiency model from eddy covariance flux data for predicting daily gross primary production across biomes. Agric For Meteorol 143:189–207. https://doi.org/10.1016/j.agrformet.2006.12.001

Zhao T, Brown DG, Bergen KM (2007) Increasing gross primary production (GPP) in the urbanizing landscapes of southeastern Michigan. Photogramm Eng remote Sens 73:1159–1167. https://doi.org/10.14358/PERS.73.10.1159

Zhao T, Brown DG, Fang H, Theobald DM, Liu T, Zhang T (2012) Vegetation productivity consequences of human settlement growth in the eastern United States. Landsc Ecol 27:1149–1165. https://doi.org/10.1007/s10980-012-9766-8